

AD-A069 169

PURDUE UNIV LAFAYETTE IND PROJECT SQUID HEADQUARTERS
CARS INVESTIGATIONS IN SOOTING AND TURBULENT FLAMES.(U)
MAR 79 A C ECKBRETH
SQUID-UTRC-5-PU

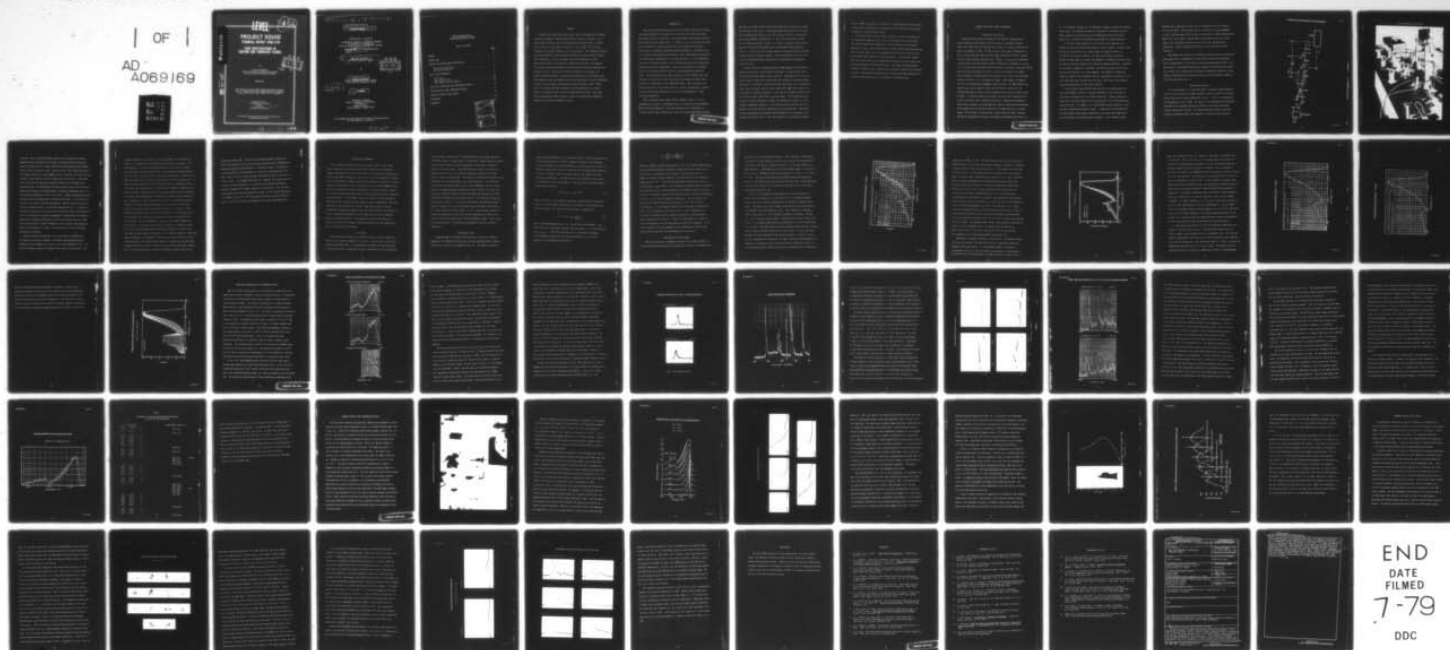
F/G 21/2

N00014-75-C-1143

NL

UNCLASSIFIED

1 OF 1
AD
A069169



END
DATE
FILMED
7-79
DDC

AD A069169

DDC FILE COPY

LEVEL

28 12

PROJECT SQUID
TECHNICAL REPORT UTRC-5-PU
CARS INVESTIGATIONS IN
SOOTING AND TURBULENT FLAMES

BY

ALAN C. ECKBRETH
UNITED TECHNOLOGIES RESEARCH CENTER
EAST HARTFORD, CONNECTICUT 06108

MARCH 1979

Project SQUID is a cooperative program of basic research relating to Jet Propulsion. It is sponsored by the Office of Naval Research and is assisted by Purdue University through Contract N00014-75-C-1143, NR-098-038.

Published for ONR by
School of Mechanical Engineering
Chaffee Hall
Purdue University
West Lafayette, Indiana 47907

403617

This document has been approved for public release and sale;
its distribution is unlimited

DDC
RECEIVED
MAY 30 1979
BULLITT
C

79 05 29 080

9 Technical rept. 1 Oct 77-28 Feb 79,

14 SQUID -
Technical Report UTRC-5-PU

P R O J E C T S Q U I D

A COOPERATIVE PROGRAM OF FUNDAMENTAL RESEARCH
AS RELATED TO JET PROPULSION
OFFICE OF NAVAL RESEARCH, DEPARTMENT OF THE NAVY

CONTRACT NO. ~~14~~ 14-75-C-1143 / NR-098-038

15

6 CARS INVESTIGATIONS IN
SOOTING AND TURBULENT FLAMES .

by

D D C
RECEIVED
MAY 30 1979
C

10

Alan C. Eckbreth

United Technologies Research Center
East Hartford, Connecticut 06108

12 67p

11

March 1979

Published for ONR by
School of Mechanical Engineering
Chaffee Hall
Purdue University
West Lafayette, Indiana 47907

This document has been approved for public release and sale;
its distribution is unlimited

403 617

Glu

CARS Investigations in
Sooting and Turbulent Flames

TABLE OF CONTENTS

	<u>Page</u>
SUMMARY	1
INTRODUCTION	3
COHERENT ANTI-STOKES RAMAN SPECTROSCOPY	7
Theoretical Description	7
Experimental Apparatus	9
CLEAN FLAME THERMOMETRY	15
Flat Flames	15
CARS Computer Code	16
CARS Temperature Measurements	18
LASER-SOOT INTERACTION AND INTERFERENCE EFFECTS	29
LAMINAR SOOTING FLAME TEMPERATURE MAPPING	45
TURBULENT SOOTING FLAME STUDIES	55
CONCLUSIONS	63
REFERENCES	65

ACCESSION for	
NTIS	White Section <input checked="" type="checkbox"/>
DDC	Blue Section <input type="checkbox"/>
UNANNOUNCED	<input type="checkbox"/>
JUSTIFICATION	
BY	
DISTRIBUTION/AVAILABILITY CODES	
Doc	SPECIAL
A	

SUMMARY

Coherent anti-Stokes Raman spectroscopy (CARS) investigations in sooting, laminar and turbulent, propane-fueled diffusion flames are reported. For a 5320 Å pump wavelength, using a frequency-doubled neodymium laser, interferences can occur at very high soot densities. For N_2 CARS, there are both incoherent and coherent components to the interference. The incoherent interference arises primarily from anti-Stokes fluorescence from C_2 excited by Stokes laser absorption. The C_2 is created by the laser vaporization of soot particulates, shown to occur even on a nanosecond time scale. The coherent interference arises most probably from electronically-resonantly enhanced wave mixing in the C_2 . Fortunately, neither interference is very large. By proper experimental design, interference-free CARS spectra from flame N_2 have been employed to map the temperature field with high spatial precision throughout a small, luminous, highly sooting laminar propane diffusion flame. Single pulse (~ 10 nanosecond) CARS thermometry has been demonstrated in various regions of a highly swirled, turbulent propane diffusion flame. Based upon these investigations, CARS continues to appear very promising for diagnostic application to practical combustion sources.

INTRODUCTION

Laser light scattering and wave mixing spectroscopic techniques are being increasingly applied to the diagnosis of the hostile, yet easily perturbed, environments typical of combustion. Spontaneous Raman scattering has received much attention in this regard (Ref. 1). However, it is a very weak process and quite susceptible to naturally occurring or laser induced interferences. Specifically, in attempting spontaneous Raman thermometry in the primary zone of a turbulent hydrocarbon-fueled combustor, severe laser-induced interferences were encountered in experiments at our laboratory (Ref. 2). The interference arises due to the laser heating of soot particulates and has been termed laser modulated particulate incandescence. Hot soot particulates are the primary cause of the broadband radiation emitted by hydrocarbon-fueled diffusion flames. The soot particles are highly absorbing to laser radiation and, when irradiated with the pulsed laser fluxes typical of diagnostic applications, are driven to temperatures in the 4000-5000°K range. Due to the acute temperature sensitivity of the Planck function, the soot incandescence is greatly increased by the laser modulation and is a serious interference in light scattering diagnostics.

Under a previous Project SQUID contract (8960-20) (Refs. 3, 4) this phenomenon was studied in considerable detail in conjunction with spontaneous Raman scattering diagnostics. The laser modulated soot incandescence is in phase with the laser radiation and, thus, the instantaneous Raman processes,

PRECEDING PAGE BLANK

and there is no phase behavior which can be exploited to increase the signal-to-interference (S/I) ratio. It was demonstrated that the S/I does increase with increasing laser flux, but the flux, and hence the S/I, is constrained due to gas breakdown considerations. It was finally concluded that when the soot densities become too high, i.e., typical of practical device levels, that the S/I would be unacceptably low for spontaneous Raman diagnostics (Ref. 5). It was clear that stronger diagnostic techniques would be required to probe practical combustion devices. This is becoming all more the situation with increasing emphasis being placed on alternative, and generally, less clean fuels.

Coherent anti-Stokes Raman spectroscopy (CARS) appears as an attractive approach for practical flame diagnosis based upon its strong signal conversion efficiencies and coherent signal character. CARS signal levels are often several orders of magnitude stronger than those produced by spontaneous Raman scattering. Its coherent, laser-like character means that all of the generated signal can be collected, and over such a small solid angle that collection of interferences is greatly minimized. At the time of our proposal (January 1977) its use had not been demonstrated in sooting flames. The investigations described herein were undertaken to examine the feasibility of CARS for sooting, turbulent combustion diagnostics. Interferences were encountered, but these were not very severe and were suppressible as will be described. Suppression of these interferences has permitted CARS thermometry to be performed in the presence of high soot levels. The other jeopardy to the successful implemen-

tation of CARS is the effect of turbulence. CARS generation has been studied in the presence of turbulence and single pulse CARS thermometry has been demonstrated in a highly turbulent flame.

In the next section of this report, CARS will be briefly discussed and the experimental apparatus used in these investigations will be described. Then CARS thermometry investigations in "clean" flames will be presented. Subsequent to that, initial CARS studies in highly sooting flames are reported, which, by their nature, led to an examination of laser-soot interaction and interference effects which will then be presented. In our earlier contract work, these were studied in the submicrosecond region; now these studies have been performed with 0 (10^{-8} second) pulses. Then temperature measurements throughout a highly sooting, laminar propane diffusion flame will be presented. The report concludes with a demonstration of single pulse CARS generation in a turbulent flame and the effects of turbulence on CARS generation.

COHERENT ANTI-STOKES RAMAN SPECTROSCOPY

Theoretical Description

Publications describing investigations into CARS are appearing at an ever-increasing rate and several very good reviews have appeared recently (Refs. 6-8), which are well referenced and to which the reader is referred for detailed treatments of CARS. In CARS, incident laser beams at frequencies ω_1 and ω_2 (often termed the pump and Stokes beams respectively) interact through the third order nonlinear susceptibility, $\chi_{ijkl}^{(3)}(-\omega_3, \omega_1, \omega_1, -\omega_2)$ to generate a polarization field which produces coherent radiation at frequency $\omega_3 = 2\omega_1 - \omega_2$. It is for this reason that CARS is often referred to as "three or four wave mixing". When the frequency difference $(\omega_1 - \omega_2)$ is close to the frequency of a Raman active resonance, the magnitude of the radiation at ω_3 , then at the anti-Stokes frequency relative to ω_1 , can become very large. Large enough, for example, that with the experimental arrangement described herein, the CARS signals from room air N_2 or O_2 are readily visible. By third order is meant that the induced polarization exhibits a cubic dependence on the optical electric field strength. In isotropic media such as gases, the third order susceptibility is actually the lowest order nonlinearity exhibited. Temperature measurements derive from the shape of the CARS spectrum. Species concentration measurements are performed from the absolute intensity of the CARS signal or, in certain ranges, from the shape of the spectrum, a unique feature of CARS. The CARS spectrum can be generated piecewise by scanning a narrowband Stokes source at

ω_2 . For diagnostic purposes, it is preferable to employ a spectrally broadband Stokes laser. This approach obviates the requirement to frequency scan the Stokes component and generates the entire CARS spectrum with each pulse, permitting, in principle, instantaneous measurements of medium properties.

For efficient signal generation, the incident laser beams must be so aligned that the three wave mixing process is properly phased. In gases, phase matching is achieved when the ω_1 and ω_2 beams are aligned coaxially or collinearly. Collinearity, however, can lead to poor spatial resolution. Because the CARS signal is coherent and undergoes an integrative growth process, the spatial resolution cannot be well defined by imaging techniques. Depending on the specific diagnostic circumstance, the spatial resolution may be worse than that desired (Ref. 9) or even ambiguous. For example, in probing hot flames surrounded by low temperature regions, significant contributions to the total CARS signal may originate from the cooler, high density outer regions, preventing measurements at the desired location.

To avoid beam overlap and three wave mixing in all regions except the desired measurement location, it would be desirable to cross the beams so that CARS is generated only at the beam intersection. Merely crossing the beams results in phase mismatch and a sharp decrease in the CARS signal generating efficiency. For example, a 1° crossing angle results typically in over an order of magnitude decrease in signal. A method has been developed (Ref. 10) which permits large angular separations of the input laser beams while still satisfying the phase-matching requirement. In this approach termed

BOXCARS, the ω_1 pump beam is split into two components which are crossed at an arbitrary angle. The ω_2 Stokes beam is introduced at an angle dependent on the ω_1 crossing angle and the molecule being probed to produce phase-matched CARS at yet a third angle. Because CARS is generated only where all three beams cross, the spatial resolution can be quite fine, and importantly, unambiguous. Spatial resolutions are similar to those achieved in laser anemometry.

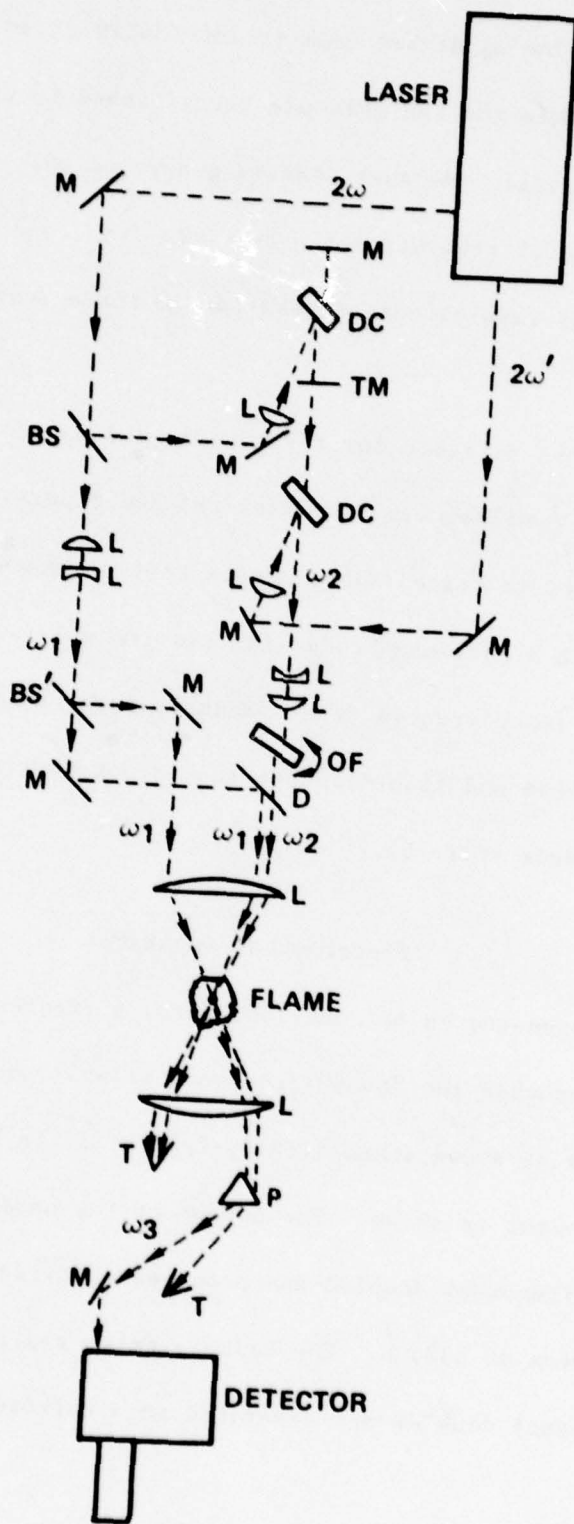
CARS appears most suitable for thermometry and major species concentration measurements and is complementary to laser-induced fluorescence approaches which are appropriate to trace radical concentration measurements (Refs. 5,11). Calculations of CARS signal magnitudes for commercially-available laser equipment indicate that interferences from combustor background luminosity or laser induced incandescences and fluorescences should not be significant compared to the CARS signal levels (Ref. 5).

Experimental Apparatus

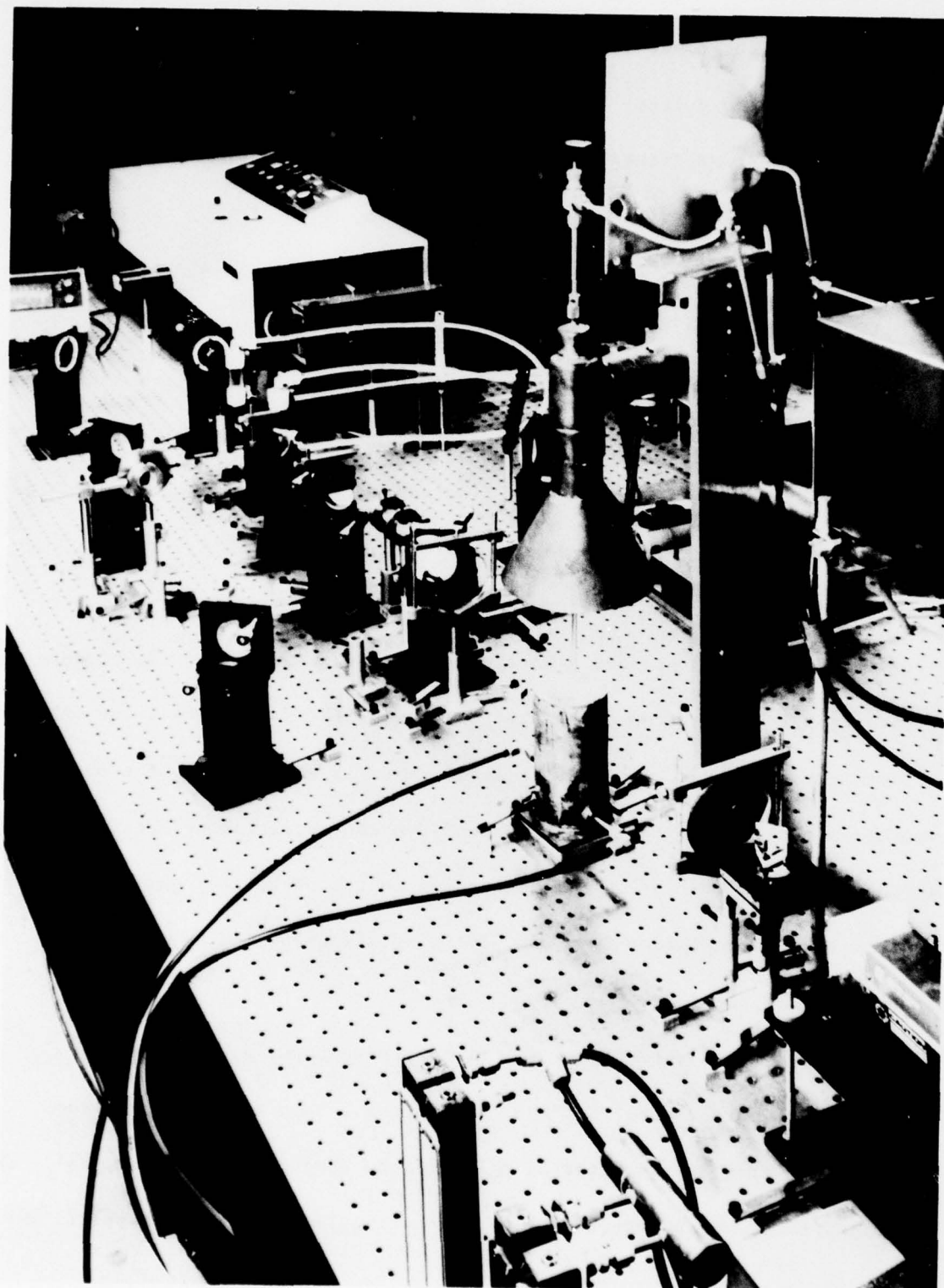
For the measurements to be described here, a frequency-doubled neodymium laser is used to provide the "pump" frequency as well as to drive the "Stokes-shifted" dye laser as shown schematically in Fig. 1. In Fig. 2 a photograph of the experimental setup is shown. The output of the neodymium laser (Quanta-Ray Model DCR-1A) is frequency doubled and produces a horizontally polarized, "primary" green beam at 5320 \AA . The primary green and residual 1.06μ upon leaving the frequency doubler are separated in a splitter section and the

UTRC BOXCARS EXPERIMENTAL ARRANGEMENT

FIG. 1



CARS EXPERIMENTAL APPARATUS



78-65-A

78 02 139 2

residual 1.06μ is frequency doubled, generating a "secondary" green beam. Depending upon the condition of the laser, the primary green is typically around 2 W (200 mJ pulses, 10 pps, 10^{-8} sec pulse duration) and the secondary about an order of magnitude lower. As seen in Fig. 1 part (about one third) of the primary is split off by the beamsplitter BS, reflected by the mirror M, and focused to pump slightly off axis a flowing dye cell oscillator. The output from the dye laser is amplified in another flowing dye cell pumped by the secondary green. The secondary green passes through a piece of KG3 air-cooled Schott glass placed at the Brewster angle to absorb any remaining 1.06μ . The dye oscillator and amplifier are in flow series. A small, magnetically-coupled, stainless steel centrifugal pump circulates the dye from a 1.5 liter reservoir through a 0.6μ filter to prevent any bubbling. The dye cells are oriented at Brewster's angle and produce a horizontally polarized output. To produce the broadband, Stokes-shifted, dye laser output desired for single pulse CARS work, a flat-flat Fabry Perot oscillator arrangement is employed and the bandwidth is appropriately centered by proper dye and dye concentration selection. Bandwidths vary from 100 to 200 cm^{-1} depending on the oscillator pump energy and whether the dye amplifier is used. By using mixtures of dyes, very broad bandwidths are obtained.

Figure 1 shows the disposition of the three beams at frequencies ω_1 , ω_1 , and ω_2 as utilized for BOXCARS. The primary pump beam after passing through the first beamsplitter is split at the second beamsplitter, BS'. The reflected component passes to the beam crossing lens via the mirror M. The

transmitted component is directed to the lens by means of a mirror and the dichroic, D, through which the Stokes-shifted dye laser at ω_2 passes. All three beams ω_1 , ω_1 and ω_2 are aligned parallel to each other in a single plane and sent to the beam crossing lens. If the beams are aligned parallel, they will cross at the focal point of the lens by definition. However, due to wavefront sphericity, they may not necessarily waist at the crossing point. To ensure that the beam waist occurs at the crossing point, adjustable telescopes are added in each leg as shown. At the high laser intensities employed, the beams are readily visualized near the focal region from the room air Rayleigh scattering. The telescopes are then adjusted to visually produce waisting at the crossing point. Also inserted in the ω_2 leg is a rotatable optical flat. Rotation of the flat permits displacement of the ω_2 beam on the focusing/crossing lens permitting the phase-matching angle, θ , to be varied. After passing through the crossing point, the four beams, i.e., CARS @ $\omega_3, \omega_1, \omega_1, \omega_2$, are recollimated by a second lens, generally the same focal length as the focusing lens. Two of the components, ω_1 and ω_2 , are trapped although they could be sent to a reference leg if desired to generate a normalizing signal. At the small crossing angles usually employed for BOXCARS, the CARS and one pump beam, although angularly separated, are not spatially separated. Additional angular separation is achieved with a double extra dense flint prism. After a suitable distance, the remaining pump component is trapped and the CARS passes through cutoff filters prior to analysis by a 1-m double monochromator (Ramanor HG2S, Jobin Yvon) fitted with an optical multichannel analyzer (SIT, silicon

intensified target, PAR). The optical multichannel analyzer captures the entire CARS spectrum with each pulse greatly expediting signal averaging and permitting single pulse measurements. In situations where it is desired to scan the spectrum, the monochromator is fitted with a photomultiplier tube whose output is fed to a boxcar averager (PAR 162/164) which in turn drives a chart recorder. In broadband CARS either the linewidth of the pump laser, the resolution of the spectrometer, or crosstalk on the optical multichannel analyzer determine the ultimate resolution of the spectrum. The 1-m double monochromator has a limiting resolution of about 0.5 cm^{-1} and the pump laser a linewidth of $\sim 0.8 \text{ cm}^{-1}$. The CARS spectral resolution was thus limited to about 0.8 cm^{-1} which is more than adequate for most gas phase diagnostics.

CLEAN FLAME THERMOMETRY

Unlike spontaneous Raman spectra which depend linearly on and, hence, mirror quantum state population distributions, CARS spectra are much more complex representative of the nonlinear nature of the three-wave mixing process. Although some simple schemes were first proposed to derive temperature information from CARS spectra, computer modeling will probably be required for accurate temperature measurements. This is particularly true for CARS thermometry from molecules with small rotational line separation. In such instances, interference effects between neighboring lines are significant and difficult to approximate analytically. In an attempt to assess the accuracy of CARS thermometry, CARS spectra were recorded from flat flames at various temperatures. The flame temperatures were obtained over a limited range from radiation corrected thermocouple readings; the radiation corrections were obtained via sodium line reversal temperature measurements on the flames near the actual conditions used for the CARS experiments. The temperature from the CARS spectra was ascertained from the best computer synthesized spectral fit and compared with the corrected thermocouple reading.

Flat Flames

Premixed flames of CH_4/air were studied over burner surfaces consisting either of a 2.5 cm dia. hexagonal or 7.5 cm dia. circular array of 0.30 cm dia. stainless steel hypo tubes. For approximately the same total mass flow rates, the two burners ran at considerably different temperatures due to the difference

in the volumetric heat release. Air flowrates were in the range from 200 to 320 cm³/sec, CH₄ in the range from 19 to 28 cm³/sec. Temperatures were measured with fine wire Pt/Pt-10 percent Rh thermocouples coated with a 90 percent Y₂O₃-10 percent BeO coating. Two thermocouples were used, one 0.0762 cm in diameter, the other 0.127 cm; each with appropriate radiation corrections agreed in regard to temperatures. The radiation corrections were obtained from sodium line reversal measurements of the flame temperature. The sodium was injected into the flame through a center tube by bubbling either the fuel/air mixture or nitrogen through a saturated salt water solution. The choice of which gas to bubble through the solution was based upon minimizing the flame temperature perturbation of the sodium injection. The temperature change was typically less than 25 K. Line reversal measurements were performed using a tungsten filament source and a 1/2-m Jarrell Ash monochromator and observing the normal cautionary procedures (Refs. 12, 13). The discrepancy between the thermocouple indication and the line reversal temperature was taken as the radiation correction and used over a limited temperature range, ~ ±50 K, about the calibration point. Corrections were determined at several different temperatures.

CARS Computer Code

A computer model to synthesize CARS spectra as a function of density, temperature and background susceptibility has been formulated under corporate funding by R. J. Hall of our laboratory (Ref. 14). The model is currently

capable of generating N_2 , CO , O_2 , H_2O and H_2 spectra. Upon inputting selection of the molecular species of interest together with density and temperature, the model calculates the state populations $n_{v,J}$ and energies, $h\nu_{v,J}$, where h is Planck's constant and v,J are the vibrational and rotational quantum numbers for the state of interest. Next the program computes the complex third order nonlinear susceptibility. The CARS radiation is proportional to the square of the absolute value of susceptibility. The third order nonlinear susceptibility may be written as

$$\chi^{(3)} = \sum_j (\chi' + i\chi'')_j + \chi^{nr} \quad (1)$$

where $(\chi' + i\chi'')_j$ is the resonant susceptibility associated with transition j and χ^{nr} is the nonresonant susceptibility contribution of the electrons and remote resonances. The resonant contribution may be expressed as

$$(\chi' + i\chi'')_j = K_j \frac{\Gamma_j}{2\Delta\omega_j - i\Gamma_j} \quad (2)$$

where the detuning frequency $\Delta\omega_j = \omega_j - (\omega_1 - \omega_2)$ has been introduced. ω_j is the frequency of a particular possible transition from $v,J + v',J'$ and equal to $|\omega_{v,J} - \omega_{v',J'}|$. Selection rules govern which transitions are allowed. Γ_j is the Raman linewidth for the transition denoted by j . K_j is the modulus of the susceptibility and equal to

$$K_j = \frac{2c^4}{\hbar \omega_2^4} n \Delta_j g_j \left(\frac{\partial \sigma}{\partial \Omega} \right)_j \frac{1}{\Gamma_j} \quad (3)$$

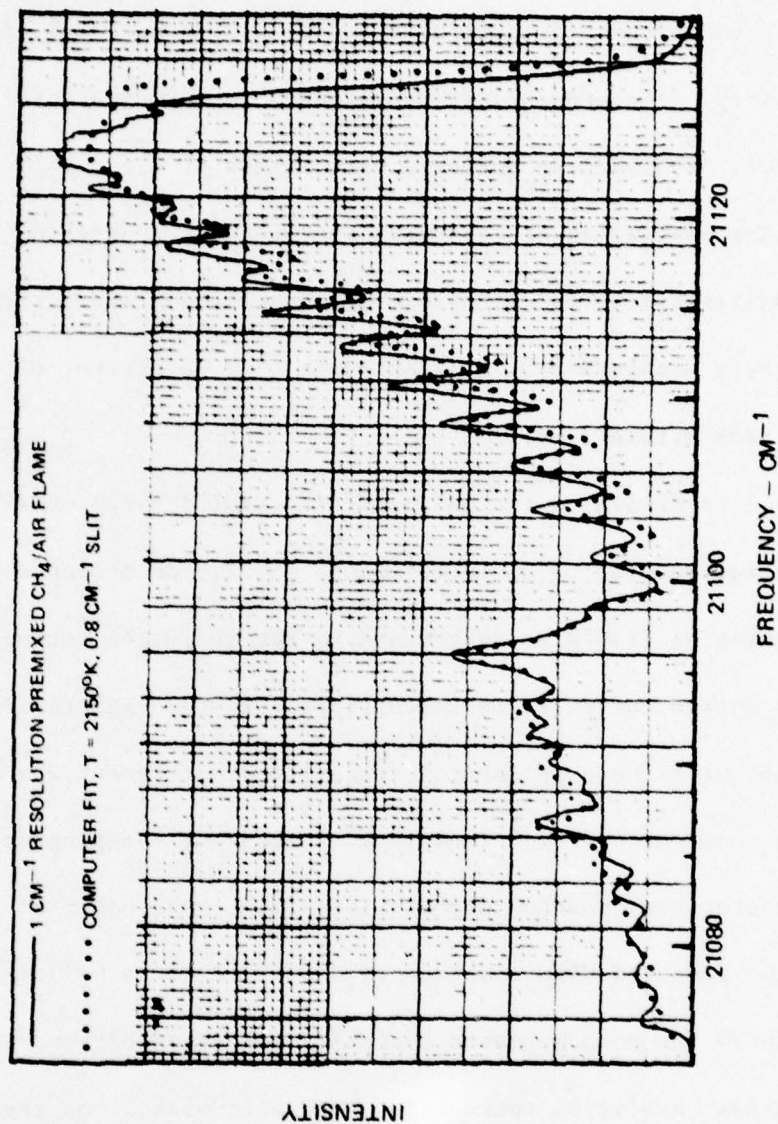
where \hbar is Planck's constant divided by 2π ; n , the total species number density; Δ_j , the normalized population difference between the levels involved in the transition; g_j , linestrength factor equal to (v_j+1) ; and $(\partial \sigma / \partial \Omega)_j$, the Raman cross section for the transition. The susceptibility is calculated by summing over all approximately allowed transitions and selecting a value for the nonresonant susceptibility. The susceptibility emerges from this subroutine as a function of $\omega_1 - \omega_2$. Next the square of the absolute value of the susceptibility is calculated together with a convolution over the function $g(\omega_1)^2 g(\omega_2)$, where $g(\omega_i)$ is the laser lineshape at frequency ω_i . This accounts for the scaling of the CARS radiation as $I_1^2 I_2$ where I_i is the laser intensity at frequency ω_i . In the program, Gaussian fits to the laser lineshapes are used. The ω_1 halfwidth varies between 0.04 to 1.2 cm^{-1} depending on the oscillator configuration and ω_2 linewidth appropriate to the experimental value, typically 125 to 300 cm^{-1} . Finally the CARS spectrum is convoluted over a monochromator slit function, generally taken to be triangular. At the display terminal, plots are available of the susceptibility, and the CARS spectrum before and after the monochromator slit convolution.

CARS Temperature Measurements

CARS spectra from N_2 in atmospheric pressure, flat flames sustained on the previously described burners were obtained by scanning the broadband CARS

spectrum with the 1-m double monochromator. Since nitrogen is the dominant constituent in air-fueled combustion processes and is present in large concentrations despite the extent of chemical reaction, it is an ideal candidate for CARS thermometry. Measurements were typically performed about 1.3 cm above the burner surface. BOXCARS was employed with angles of $\alpha = 2.14^\circ$, $\theta = 2.5^\circ$ and $\phi = 1.95^\circ$. The spatial resolution was determined by generating CARS from within a translatable 0.015 cm thick microscope slide cover. Signal generation occurred entirely within a 0.5 cm extent with over 90 percent of the signal originating from within 3 mm.

In Fig. 3 is displayed the CARS spectrum (solid line) obtained at a nominal spectral resolution of 1 cm^{-1} above the 2.5 cm diameter hexagonal burner operating at 2110°K as determined by the radiation corrected thermocouple. The dotted curve is the computer synthesized spectrum which gave the best agreement with the experimental trace. Best agreement was obtained at 2150°K using constant 0.1 cm^{-1} linewidths throughout the program. Variable (i.e., with rotational quantum number) linewidths have not been studied as yet. In Fig. 3, the computed CARS spectrum is displayed for a 0.75 cm^{-1} monochromator resolution. The monochromator typically possesses better spectral resolution than the nominal resolution indicated by the slit width. As seen, very good agreement with the experimental trace has been obtained. In the $0 + 1$ band, the low J Q-branches are unresolved. At higher rotational quantum numbers, the splitting of the band due to the vibration-rotation interaction, $a_e J(J + 1)$, is sufficiently large to permit the resolution of individual even J Q-branches,

FLAME N₂ BOXCARS SPECTRUM, T = 2110°K

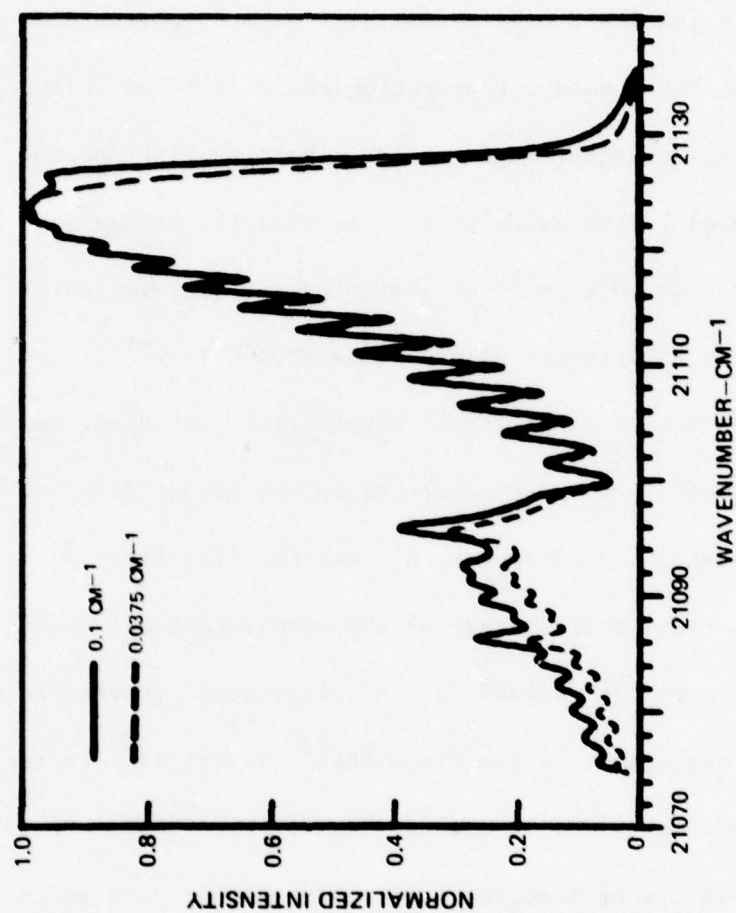
ranging from Q (28) to Q (40). The odd Q-branches, which have a nuclear spin weighting equal to half of the even-numbered branches, are reduced in intensity by about a factor of four and do not stand out. For Q-branches beyond Q (40), overlap with the $1 + 2$ band transitions occurs, giving rise to two prominent peaks in the "hot" band. Reproducing these features in the computer spectrum places stringent requirements on the vibrational-rotational energy level positions used in the calculation. Because the homogeneous linewidths are expected to be 0 (0.1 cm^{-1}) or less, the energy level positions must be calculated to an accuracy of much less than 0.1 cm^{-1} if these spectral coincidences are to be predicted accurately. The predicted hot band features have been found to be very sensitive to the values selected for the vibration-rotation interaction parameter, α_e , and the line positions $v = 0, 1$, and 2 . It has been found that the use of the more recent α_e values (Refs. 15, 16) in conjunction with the various sets of vibrational anharmonic constants (Refs. 17, 18) or measured line positions (Ref. 19) all fail to reproduce the observed spectral overlaps. The agreement shown in Fig. 3 was obtained by employing the α_e and ω_{01} values of Bendtsen (Ref. 15) together with an adjusted ω_{02} value of 4631.34 cm^{-1} . This value is within 0.05 cm^{-1} of that inferred from examination of the Lyman-Birge-Hopfield system (Ref. 20).

Broadening of the Raman Q-branches is mainly due to rotationally inelastic collisions and therefore the cross section may be a complicated function of temperature and concentration. In the foregoing computer calculation, a J-independent value of 0.1 cm^{-1} was employed as mentioned. An indication of the sensitivity of these predictions to assumed linewidth is shown in Fig. 4

FIG. 4

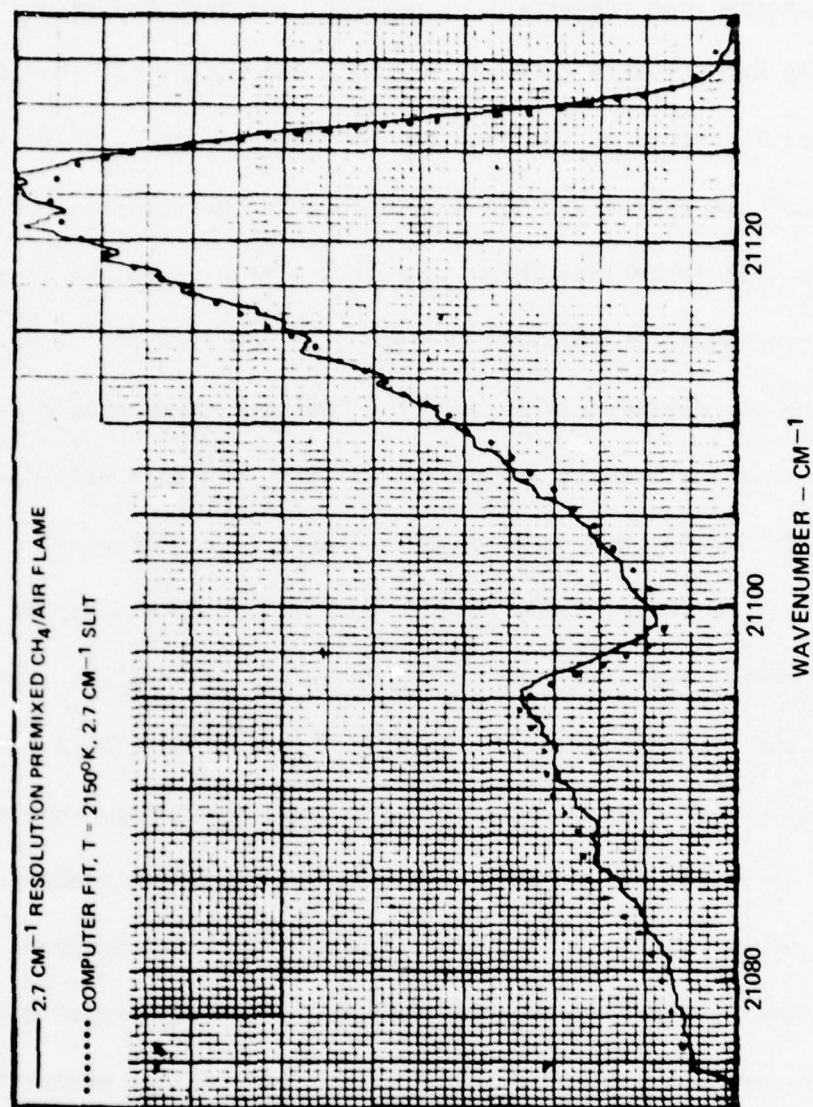
LINEWIDTH SENSITIVITY OF N₂ CARS SPECTRA

T = 2150°K, 0.8 CM⁻¹ SLIT



where the calculation of Fig. 3 is compared to one based on a linewidth value of 0.0375 cm^{-1} . This is the value of the linewidth that results from $T^{-1/2}$ scaling of the room temperature linewidth. As seen the predicted spectrum is moderately sensitive to this variation in linewidth. As the linewidth is decreased, the slope of the fundamental band hot side and the relative intensity of the hot band decrease. The discrepancy in the spectra in Fig. 3 would be worse for linewidths less than 0.1 cm^{-1} . As the linewidth is reduced, higher temperatures would be required to match the computed and experimental spectra, increasing the discrepancy between the CARS and thermocouple measurement of temperature. Furthermore, temperatures above the adiabatic flame temperature of CH_4/air , 2236°K (Ref. 21), would be required to force a fit at reduced linewidths. At larger linewidths, e.g. 0.125 cm^{-1} , a sharp peak is predicted on the $\text{N}_2 \text{ v}=0 \rightarrow 1$ bandhead which is not seen experimentally. For the flames studied, the N_2 Raman Q-branch linewidths appear to be 0 (0.1 cm^{-1}). While the sensitivity of N_2 CARS thermometry to the unknown homogeneous widths is not extreme, more information about the temperature and concentration dependences of these widths would obviously be desirable for very accurate work.

At lower spectral resolution (2.7 cm^{-1}) the individual Q-branches can no longer be resolved as seen in Fig. 5. The theoretical prediction for $T = 2150^\circ\text{K}$ is again in good agreement with the experimental trace. For these low resolution experiments, the energy level accuracy becomes much less important in fitting the theoretical to the experimental spectra. In Fig. 6 is shown the BOXCARS spectrum taken over the 7.5 cm dia. burner. The computer spectrum producing the best fit occurred at a temperature of 1650°K , in good agreement

FLAME N_2 CARS SPECTRUM, $T = 2110^\circ K$ 

FLAME N₂ BOXCARS SPECTRUM, T = 1610°K

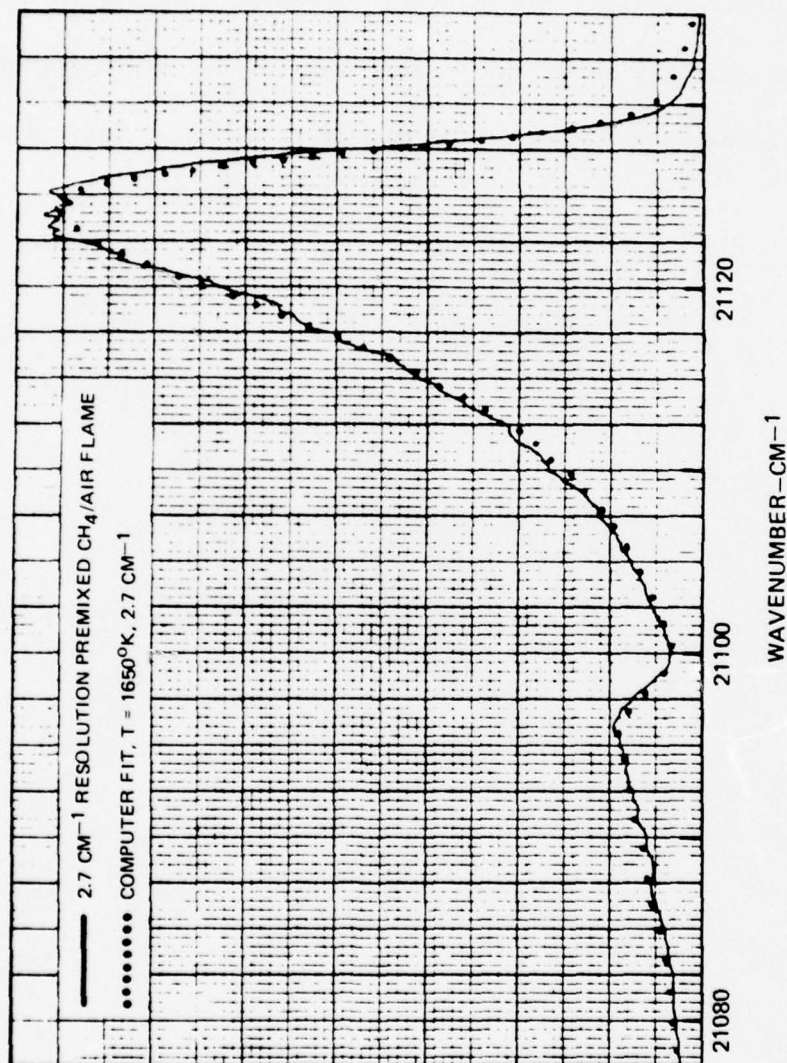


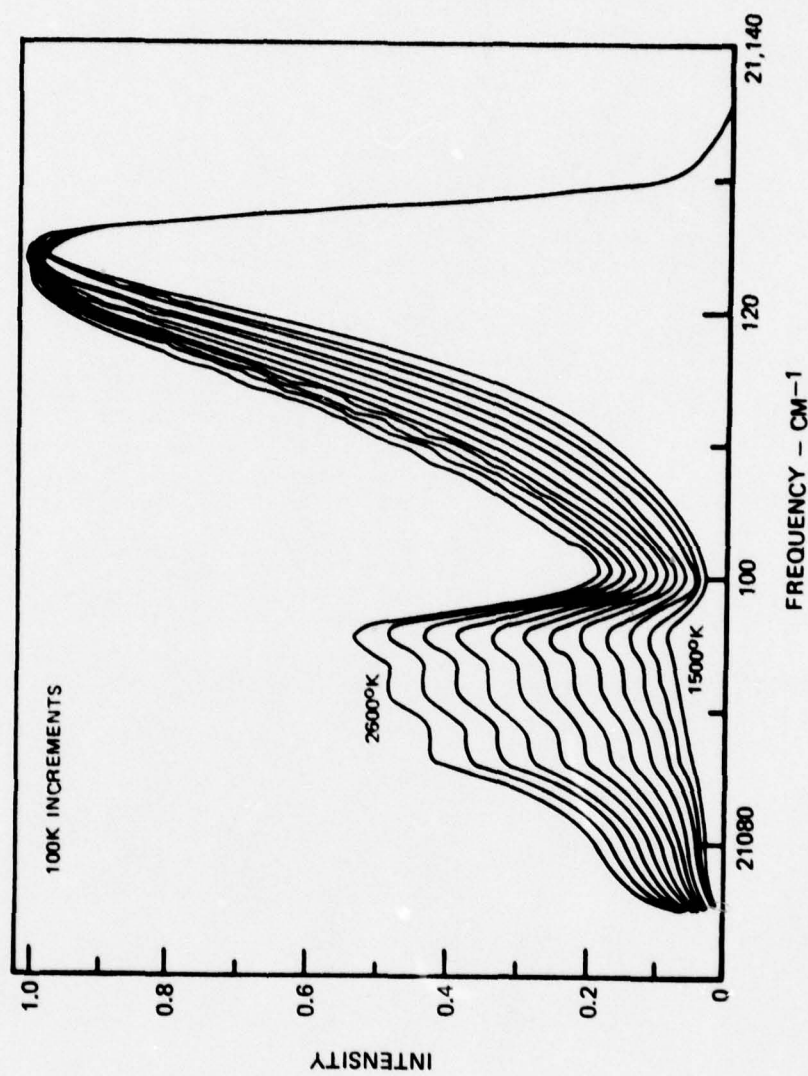
FIG. 6

with the corrected thermocouple measurements of 1610°K . As seen in Fig. 7 these lower resolution spectra are a fairly sensitive function of temperature. The width and slope of the fundamental band and the relative intensity of the hot band provide a basis for accurate thermometry at low resolution. From the computed sensitivity shown and on the basis of the above computer fitted temperature determinations, measurements appear possible at this time to within 50°K .

FIG. 7

TEMPERATURE VARIATION OF N₂ CARS SPECTRA

2.7 CM⁻¹ SPECTRAL RESOLUTION



LASER-SOOT INTERACTION AND INTERFERENCE EFFECTS

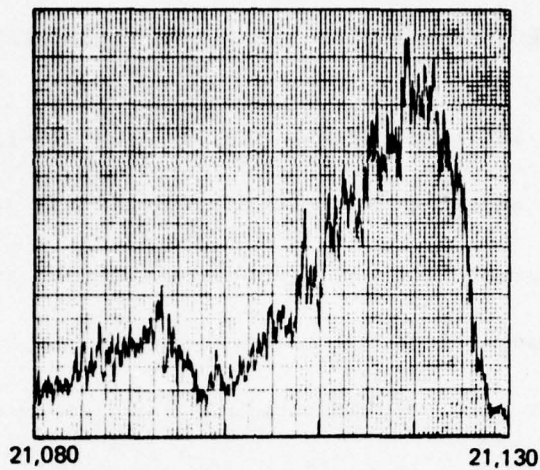
CARS is of great interest because of its potential for operation in the highly particle laden environments typical of practical devices. To investigate this potential, CARS generation was studied in laminar, sooting, methane or propane diffusion flames. Such flames were employed in our previous Project SQUID studies of laser modulated particulate incandescence interferences in Raman scattering diagnostics (Refs. 3,4). The flame is sustained on a stainless steel tube, 0.8 cm i.d., and established by merely flowing propane or methane through the tube. A coannular air flow through a concentric 1.3 cm i.d. tube is also employed to spatially stabilize the flame. The flame resembles that from a candle and is highly sooting. Mie scattering diagnostics indicated a soot number density on the order of 10^{10} cm^{-3} with an average particle diameter of 400 \AA when burning propane. This is a very high soot level producing an attenuation in transmitted light of tenths of percent per mm pathlength. The requisite spatial resolution was achieved with BOXCARS using an 89 mm dia, 305 mm focal length lens. The phase-matching angles of $\alpha=5.7^\circ$ and $\theta=6.5^\circ$ gave a resolution of approximately 0.4 mm in diameter by 1 mm long experimentally determined by generating CARS in a translatable glass slide.

In Fig. 8 are shown BOXCARS spectra (ostensibly from N_2) from laminar sooting flames employing a 270 cm^{-1} wide Stokes dye laser. In Fig. 8a is the scanned CARS spectrum at 4 cm^{-1} spectral resolution from N_2 above the luminous tip of a methane diffusion flame, i.e., above the regions of soot concentration. The spectra are hashy because no output smoothing was employed on the

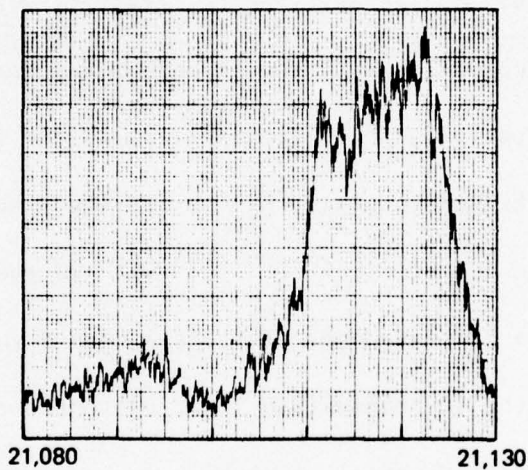
INITIAL CARS SPECTRA FROM SOOTING FLAMES

(a) CH_4 -AIR; ABOVE LUMINOUS TIP

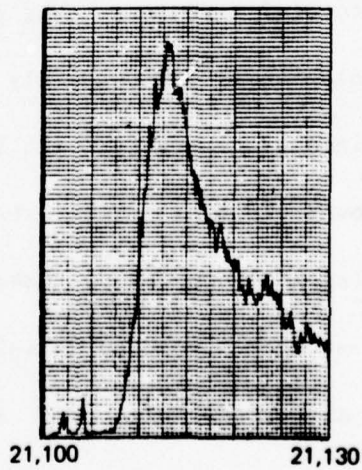
11/22/77-2c

(b) CH_4 -AIR; IN SOOT ZONE

11/22/77-2b

(c) C_3H_8 -AIR; IN SOOT ZONE

11/28/77-1

FREQUENCY - CM^{-1}

boxcar averager. The broadened ground state and hot bands typical of flame N_2 are readily apparent. In Fig. 8b the scanned CARS spectrum from within the soot zone of the methane-fueled diffusion flame is shown. Comparing Figs. 8a and 8b, a spectral interference is clearly evident in the CARS spectrum from the sooting region of the flame. In Fig. 8c is shown the spectrum obtained from within the soot zone of a propane-fueled diffusion flame. In this case the interference dominates the spectrum and there is only a slight hint of the N_2 ground state peak at $\sim 21,125 \text{ cm}^{-1}$. The interference shown in Fig. 8c consists of both incoherent and coherent features. The incoherent contribution is ascertained by blocking one of the ω_1 pump beams or, preferably, rotating the optical flat in the ω_2 Stokes beam to phase mismatch the three wave mixing process. In Fig. 8c the coherent component was about 25 percent of the total signal at the peak. In the succeeding paragraphs, the incoherent interference will be first discussed followed by a consideration of the coherent component.

The strong spectral feature seen in Fig. 8b,c arises from C_2 which has a major Swan band transition at 4737\AA ($21,110 \text{ cm}^{-1}$) midway between the N_2 ground state band peak at 4733\AA and hot band peak at 4740\AA . The Swan system arises from electronic transitions between the $A^3\Pi_g$ and $X'^3\Pi_u$ levels in C_2 and depending on the vibrational levels involved, span the visible in a well-banded structure from 4300 to 6700\AA . The Swan bands are rotationally smeared at high temperatures reflecting increasing fractional populations in higher rotational quantum number states. The band consists of strong P ($\Delta J=+1$) and R ($\Delta J=-1$) branches and a weak Q ($\Delta J=0$) branch. The band head forms by the P

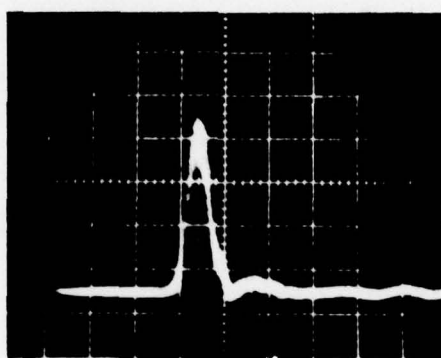
branch turning back on itself causing the band to shade or degrade to the violet (Ref. 22). As identified in our earlier studies (Refs. 3,4), the C_2 is produced by the laser vaporization of soot particulates and is one of the dominant vapor species produced. At the high laser intensities used to generate CARS, significant soot vaporization occurs even on a nanosecond time scale as seen in Fig. 9. There the monochromator signal at 4737\AA is compared with the pump laser pulse at 5320\AA . The laser pulse is approximately 10 nsec FWHM in reality, but is stretched somewhat in the photomultiplier used due to its 3 nsec rise and fall time. As seen the emission exhibits a risetime comparable to the laser pulse and is in phase with it (not clearly shown in the figure). The lack of phase lag is due to the fact that there are no effective soot heat transfer processes other than vaporization (Ref. 4) resulting in flashed vaporization of the soot surface upon pulsed laser irradiation. The emission at 4737\AA is primarily Swan emission plus a smaller laser modulated soot incandescence contribution. At other wavelengths where there are no Swan contributions, the incandescence displays similar temporal behavior. As mentioned in the introduction, because there are no phase lags to exploit in this behavior, laser modulated soot incandescence is very difficult to circumvent and presents a very serious interference to spontaneous Raman diagnostics (Ref. 5).

An optical collection system was set up at right angles to the central BOXCARS axis and the spectral behavior of the laser induced soot emissions was examined with a 0.5-meter Jarrell-Ash monochromator. In Fig. 10 is shown a spectral scan of the emissions between 6500 and 4500\AA (Ref. 23). The

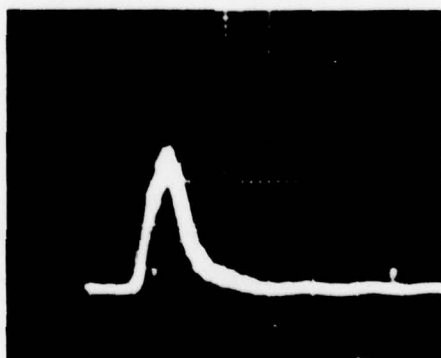
TEMPORAL BEHAVIOR OF LASER - INDUCED EMISSIONS

LASER PULSE, 5320Å⁰

11/9/78-11

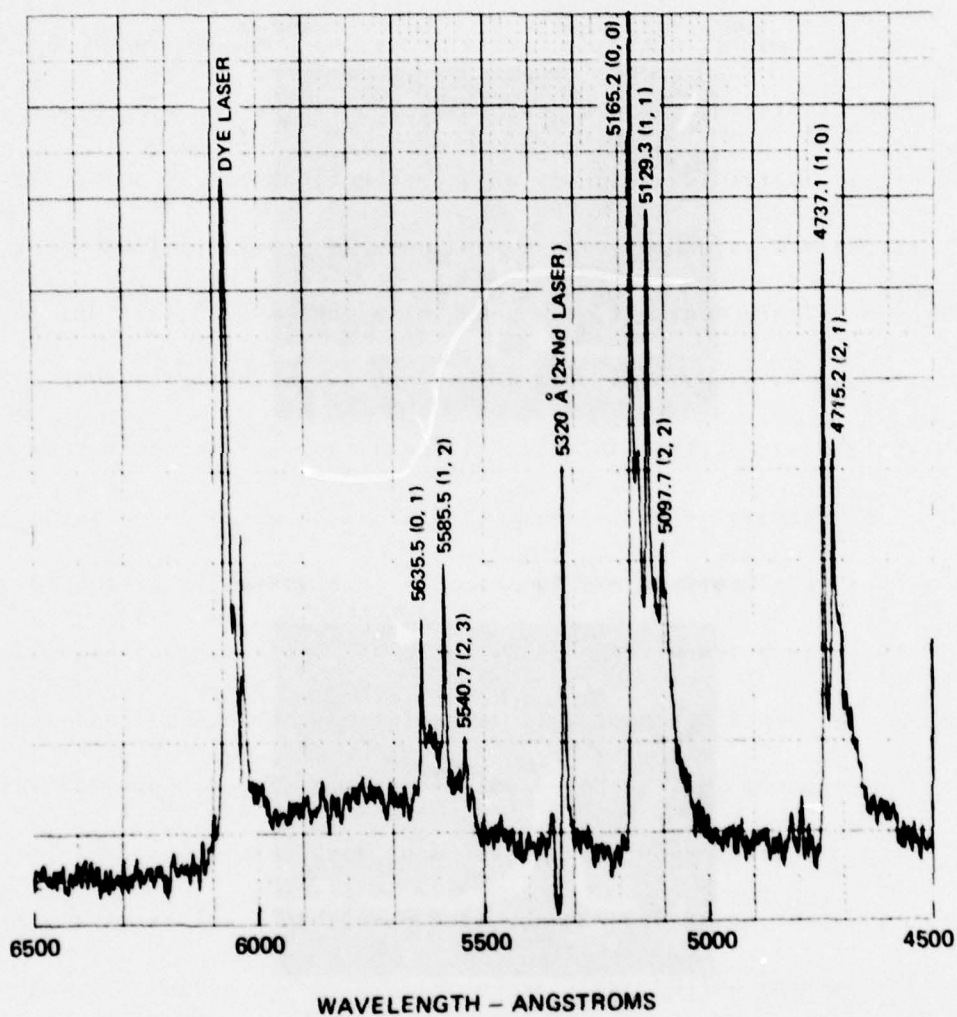
C₂ SWAN (1,0) AT 4737Å⁰

11/9/78-8a



TIME → 20 NANOSECONDS/DIV

LASER INDUCED SOOT EMISSIONS

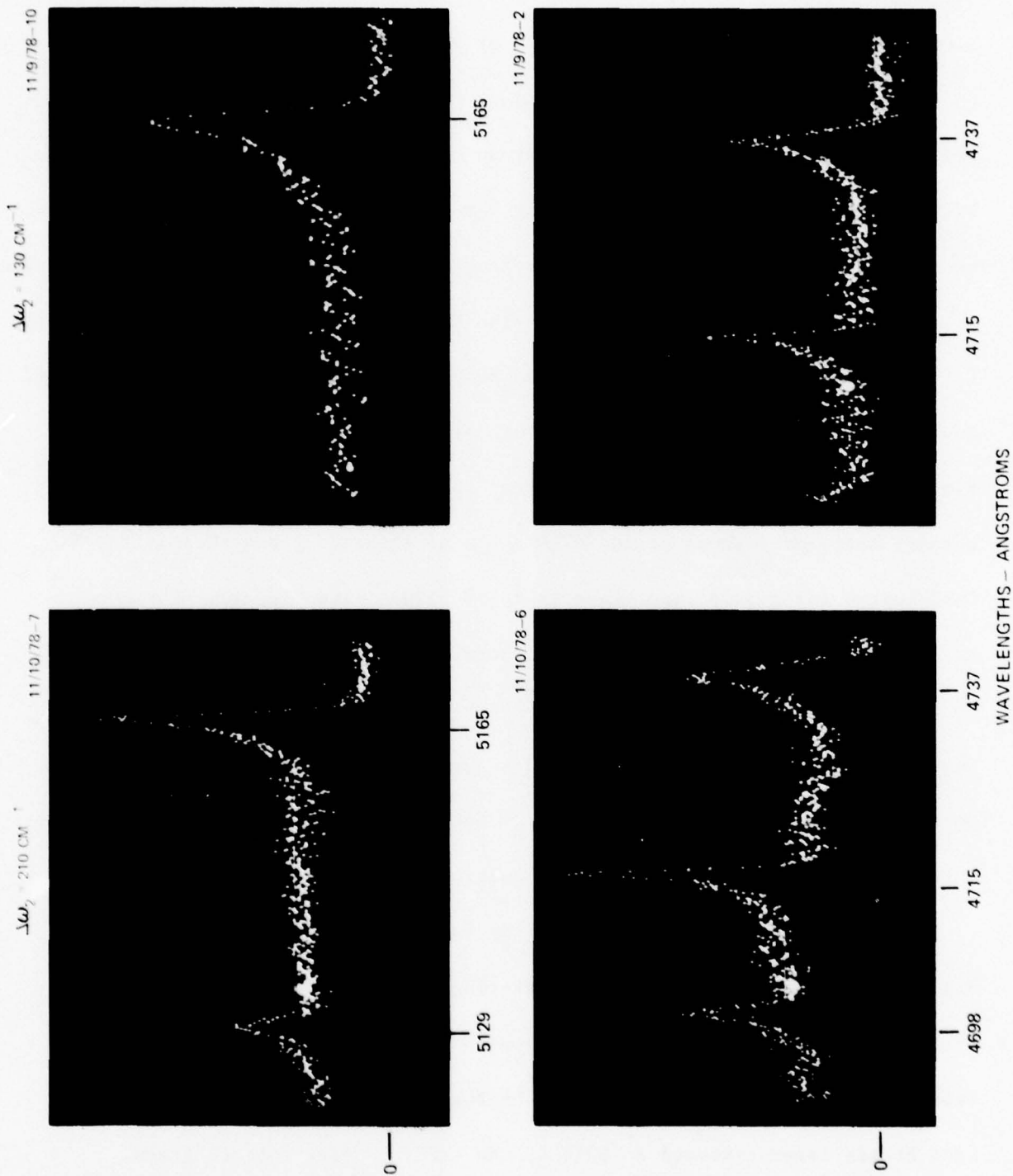


output of the spectrometer photomultiplier was fed to one channel of the boxcar averager and the monochromator scanned at $50 \text{ \AA}/\text{min}$. As seen the broad incandescence background is punctuated by the Swan bands from C_2 which rise well above the incandescence by nearly an order of magnitude in some locations. The numbers in parentheses identifying the various bandheads refer respectively to the upper and lower vibrational quantum numbers of the transition in emission.

The laser induced emissions can also be collected in the forward direction (along the central beam axis) with the BOXCARS recollimating lens and directed to the 1-m double monochrometer with mirrors or the dispersing prism. In Fig. 11 are shown the laser induced Swan bands recorded on the optical multichannel analyzer. Those around 4700 \AA are of interest since this is the N_2 CARS region for a pump laser wavelength of 5320 \AA ($2\times Nd$ laser). The band at 5165 \AA is the strongest one in the Swan system. Of note in both Figs. 10 and 11 is the spectral breadth of these bands from hot C_2 . In general, the rotational structure of each band merges together with the emission in each region spread over many tens of Angstroms. The rotational fine structure is quite evident in the optical multichannel analyzer recordings.

The emissions are quite interesting in that they display substantially different response to the exciting wavelength, which provides a clue to their origin. In Fig. 12 are displayed comparison scans of the incoherent laser induced emissions separately excited by the 5320 \AA pump laser and the broad-band Stokes laser centered at 6073 \AA . As seen the more intense green flux gives an incandescence spectrum with a very weak Swan structure superimposed.

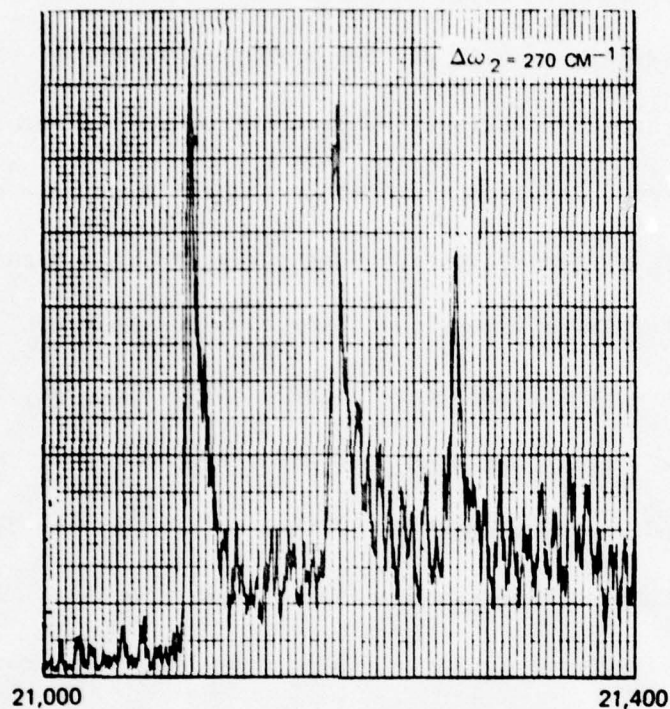
LASER INDUCED C₂ SWAN EMISSIONS



LASER-INDUCED EMISSIONS BEHAVIOR WITH EXCITATION WAVELENGTH

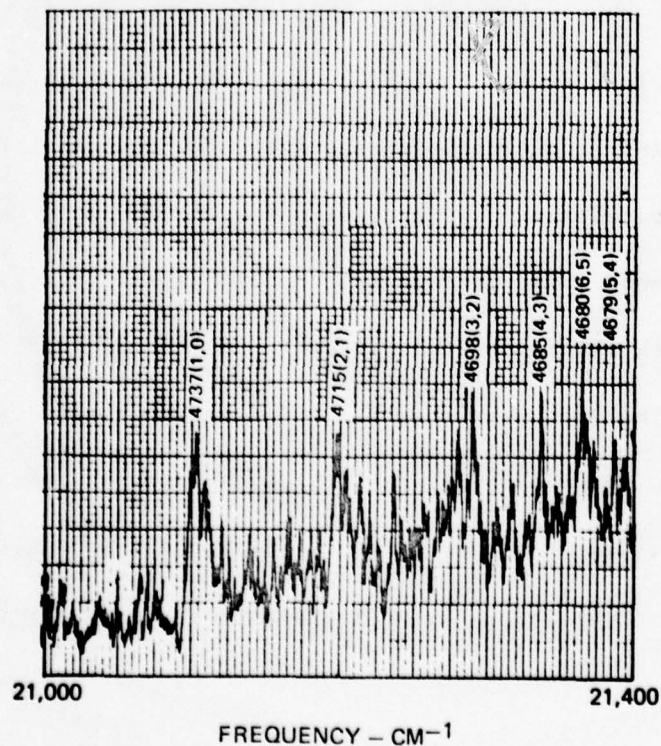
a) STOKES LASER EXCITATION

11/28/77-7a



b) 5320 Å EXCITATION ONLY

11/28/77-7b



The lower intensity, by about an order of magnitude, ω_2 beam gives a weaker continuum with very pronounced and dominant Swan structure. In addition there is an interesting synergism. At any one Swan peak location, the summation of the individually-excited contributions from the ω_1 and ω_2 beams does not equal the interference level attained with both wavelengths simultaneously present. The high intensity ω_1 beam drives the soot particles to a higher surface temperature than the lower intensity Stokes beam due to the higher flux level and produces more incandescence. The vaporization rates are also greater at the higher flux level. The weak Swan structure on top of the incandescence is most likely produced by thermal excitation of the vaporized C_2 . With the Stokes laser excitation, vigorous vaporization still occurs. But in this case, the bulk of the very strong C_2 emissions is most likely anti-Stokes fluorescence. In the region of the broadband Stokes laser centered at 6073\AA there are Swan band absorptions at the bandheads beginning at $6191.2 (2,0)$, $6122.1 (3,1)$, $6059.7 (4,2)$ and $6004.9 (5,3)$. The numbers in parentheses are again the initial and final states respectively of the transition but, now, for absorption. The absorptions are actually quite broad due to the rotational structure of the bands as described earlier. In fact in one set of experiments the Stokes bandwidth was varied from 15 cm^{-1} , to 130 cm^{-1} to 210 cm^{-1} at nearly constant energy. The Swan emissions at 4737\AA were monitored and found to scale as 1, 0.75, 0.65 respectively, indicative of a broad absorption continuum. The Swan band emissions in the vicinity of the N_2 CARS region initiate from the same states that the absorptions in the Stokes region terminate at, namely,

4737.1 (1,0), 4715.2 (2,1) and 4697.6 (3,2). The synergism described above results probably from the ω_1 laser providing a higher vaporized C_2 concentration for the ω_2 Stokes-laser induced anti-Stokes fluorescence.

As mentioned previously, the strong spectral interference displayed in Fig. 8c also contains a coherent component. There is evidence in our data that the strength of the coherent portion is stronger than what is expected from the N_2 alone in this spectral region. The additional coherent signal arises most likely from three wave mixing in the laser produced C_2 vapor which is electronically resonantly enhanced due to the coincidence of the CARS ($2\omega_1 - \omega_2$) and C_2 electronic transition at 4737.1 Å. The coherent component is, fortunately, relatively weak, i.e. $\leq N_2$ $v=0 \rightarrow 1$ CARS peak, even at very high soot densities, e.g., propane flame. At lower soot densities, e.g. methane flame, most of the coherent signal at the Swan peak appears to originate from N_2 . This is a fortuitous situation. Incoherent interferences are generally suppressible in coherent spectroscopy while coherent features are obviously more problematical.

The situation depicted in Fig. 8c is not all that formidable since the interference is fairly sharp and not very large. For high temperature measurements, the temperature can be ascertained from the ratio of the N_2 hot to ground state band heights. The C_2 bandhead is sharp and does not interfere with the weaker hot band at all. Furthermore, the C_2 band degrades toward the N_2 ground state band peak. Thus modest increases in the signal/interference ratio will improve the situation markedly. Since the CARS signal from N_2 using aligned, polarized laser sources is similarly polarized, a factor of

two discrimination against incoherent interferences is obtained by insertion of a polarization filter in the CARS detection system. By reducing the Stokes laser bandwidth from the previously employed 270 cm^{-1} (using a binary dye mixture) to $120\text{--}150\text{ cm}^{-1}$ (typical of a single dye and still adequate for broadband CARS from N_2) the CARS signal was quadrupled due to the increase in Stokes spectral power density. A factor of two was anticipated due to the reduction in bandwidth. An additional factor of two resulted because the single dye lased twice as efficiently as the binary dye combination used to achieve the very broad bandwidths. Also, as mentioned earlier, the bandwidth reduction decreases the anti-Stokes fluorescence slightly. These changes resulted in nearly an order of magnitude increase in signal to interference ratio. In so doing the spectrum shown in Fig. 13 was obtained. This BOXCARS spectrum was obtained at a nominal spectral resolution of 1 cm^{-1} from a laminar propane flame sustained on a 1.27-cm dia. tube. The CARS measurement was made on the centerline approximately midway between the inner and outer flame cones. The best computer fit (visually) is shown dotted and occurred at a temperature of 2000°K .

The situation with N_2 vis-a-vis interferences in sooting flames would appear to be almost singular. In Table I are listed the major bandheads in the Swan system together with the Stokes laser and CARS frequencies for various molecules using a 5320 \AA pump laser. As is apparent, N_2 is about the only molecule with its Stokes laser frequency in a strong Swan absorption region and its CARS frequency very near a Swan emission bandhead. The Stokes frequency

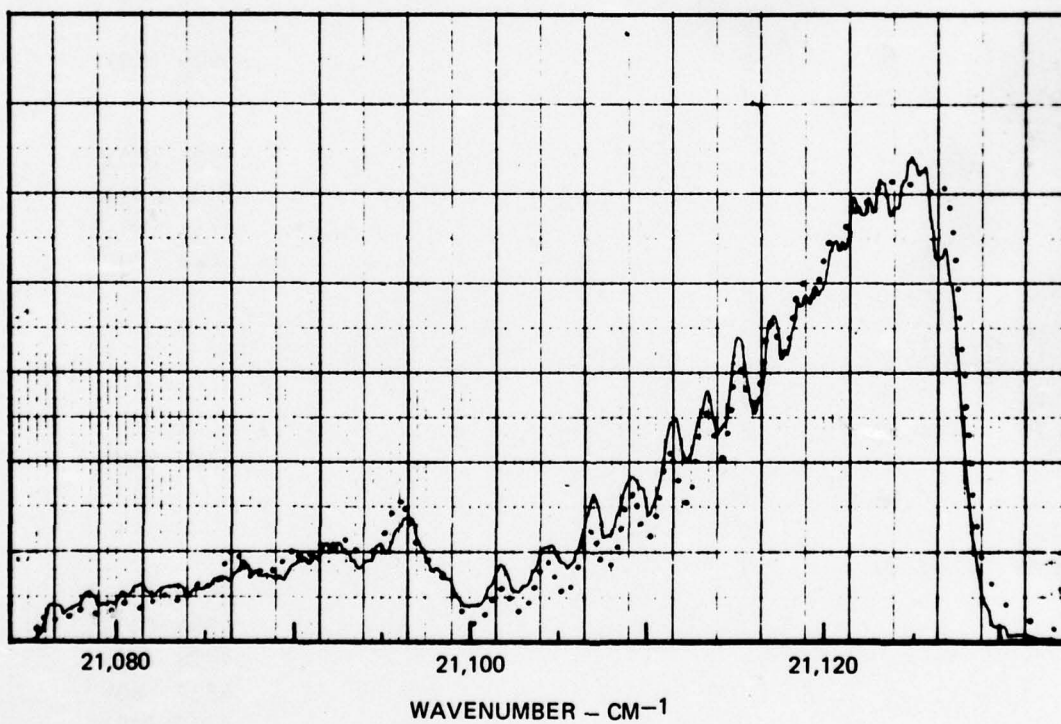
BOXCARS SPECTRUM OF N_2 IN SOOTING FLAME. COMPUTER FIT, $T = 2000^\circ K$, 0.8 CM^{-1} SLIT

TABLE I
COMPARISON OF SWAN AND CARS/STOKES WAVELENGTHS
FOR 5320 Å PUMP WAVELENGTH

<u>λ (Å)</u>	SWAN System <u>(v', v'')</u>	<u>I</u>	CARS/STOKES (Molecule)	
6677	(2, 5)	1	6836 (H ₂)	
6599	(3, 6)	1	6605 (H ₂ O)	
6534	(4, 7)	2		
6481	(5, 8)	2		
6442	(6, 9)	2		
6191	(0, 2)	3		
6122	(1, 3)	4		
6060	(2, 4)	3	6073 (N ₂)	
6005	(3, 5)	3	6005 (CO)	
5959	(4, 6)	2		
5923	(5, 7)	1		
			5901 (NO)	STOKES
			5800 (O ₂)	
			5774 (CO ₂)	
			5721 (NO ₂)	
5636	(0, 1)	8		
5586	(1, 2)	8		
5541	(2, 3)	6		
5502	(3, 4)	4		
5470	(4, 5)	2		
5165	(0, 0)	10	5320 (2xNd)	
5129	(1, 1)	6		
5098	(2, 2)	1		
			4971 (NO ₂)	
			4954 (CO ₂)	
			4913 (O ₂)	CARS
			4837 (NO)	
			4775 (CO)	
			4733 (N ₂)	
4737	(1, 0)	9		
4715	(2, 1)	8		
4698	(3, 2)	7		
4685	(4, 3)	4		
4680	(6, 5)	1		
4679	(5, 4)	2		
			4454 (H ₂ O)	
4383	(2, 0)	2		
4371	(3, 1)	4		
4365	(4, 2)	5		
			4354 (H ₂ O)	

for CO is nearly coincident with a (5,3) absorption, but the CO CARS signal is well removed from any Swan emissions. In examining Table 1, recall again that the bands degrade (i.e., spread) to the violet. H₂ CARS could suffer from thermally excited C₂ but not from anti-Stokes fluorescence, since the H₂ Stokes frequency is well beyond the high wavelength end of the strong Swan system. There are Swan absorptions beyond 7000 Å emanating from very high vibrational states, v=10,11. For CARS studies employing a ruby laser to provide the pump frequency at 6943 Å, anti-Stokes fluorescences would not be excited. Thermally excited C₂ emissions might provide some interference for weak CARS signals in the 5500-6500 Å range.

LAMINAR SOOTING FLAME TEMPERATURE MAPPING

Based upon the foregoing investigations, CARS has been employed to perform detailed axial and radial temperature surveys in the highly sooting flame shown in Fig. 14. A slow flow of gaseous propane issued through a central tube, 12.7 mm I.D., and burned in a coannular flow of air issuing from an outer tube 25.4 mm I.D. The flow speed of the propane was about 0.6 cm/sec; the mean axial flow of air was approximately 9.1 cm/sec. The air was swirled slightly to promote better spatial stability of the flame. The flame was placed in a lucite housing to eliminate unsteadiness from drafts. The flame is very luminous due to soot incandescence; the visible flame tip height is about 32 mm. BOXCARS was employed at phase-matching half angles for ω_1 of 5.7° and ω_2 of 6.5° . This gave a spatial resolution of approximately 0.4 mm in diameter by 1 mm long again experimentally measured by generating CARS in a translatable microscope slide cover. The laser beams are clearly seen crossing through the sooting flame in Fig. 14. The ω_2 beam, which resides slightly overlapped with the one ω_1 component, is not separately distinguishable. CARS spectra at various locations in the flame were averaged on the optical multichannel analyzer for 10-30 seconds depending on the CARS signal strength. Since the laser operates at 10 Hz, the spectra represent averages over 100-300 pulses. Laser induced and naturally occurring background as well as detector noise were separately averaged with one ω_1 component blocked (to exclude CARS generation) and subtracted from the accumulated signal plus background without the beam blocked.

BOXCARS THERMOMETRY IN THE SCOOTING FLAME

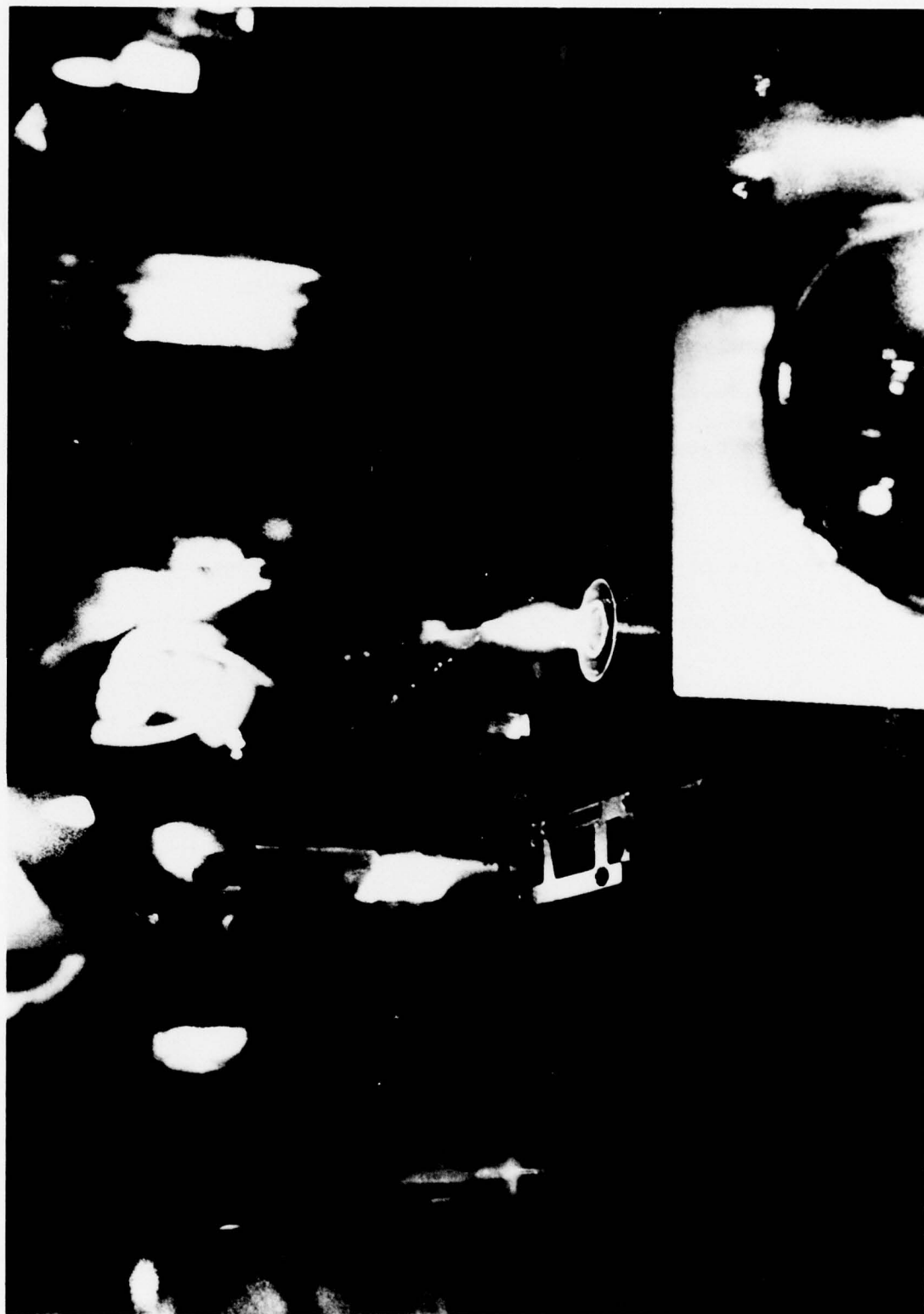


Figure 15 displays the calculated temperature dependence of the N_2 CARS spectrum computed for parameters corresponding to the experimental approach, i.e., $\Delta\omega_1 = 0.8 \text{ cm}^{-1}$, $\Delta\omega_2 = 130 \text{ cm}^{-1}$ and 1.0 cm^{-1} spectral resolution. The calculations shown in Fig. 7 were at a resolution of 2.7 cm^{-1} . In the calculations, a constant Raman linewidth of 0.1 cm^{-1} was employed. From the sensitivity of the calculated spectra and using constant linewidth codes, it appears possible at present to perform temperature measurements accurate to within 50 K at flame temperatures.

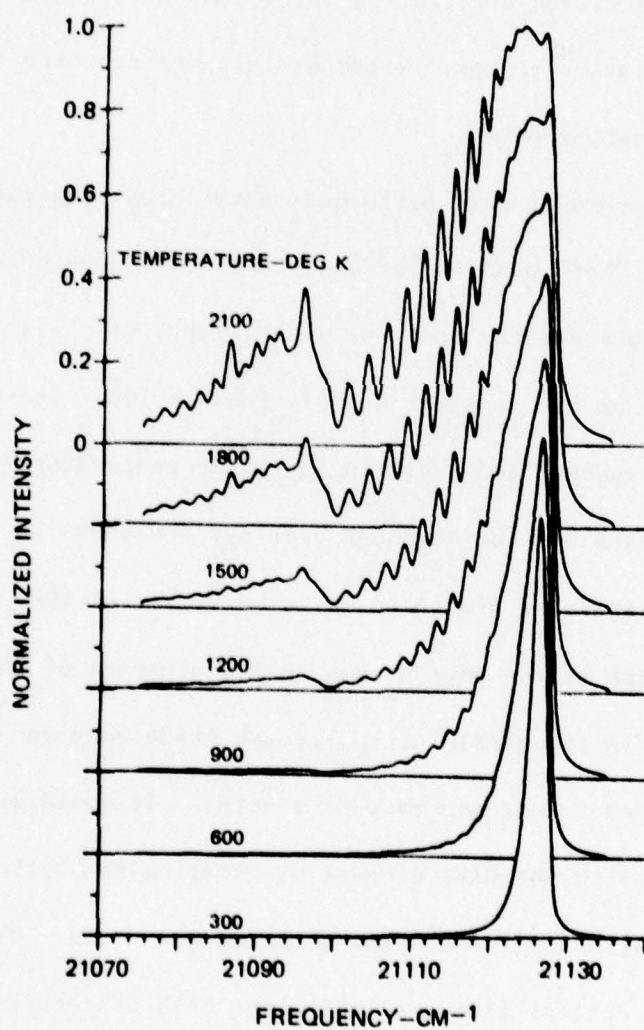
Temperature measurements were performed on the high temperature spectra from the ratio of the "hot" band to "ground state" band peak height ratio and on the lower temperature spectra from the width, FWHH, of the ground state band. Transparencies of the computer calculations in 100 K increments were also overlaid on the spectra to ascertain the flame temperature to within 50 K. Examples of the OMA data and the computer overlays are shown in Fig. 16. In Fig. 16, a-d, comparisons are presented at temperatures of 600, 1400, 1900 and 2300°K. The latter fit is the poorest due to the presence of some interference from C_2 in the middle of the ground state band and the method in which the laser induced interferences were sampled. It would have been preferable to phase mismatch the CARS process by rotating the optical flat and sampling background with all three beams striking the flame. With the aperture and thickness of the optical flat available, the CARS process could not be completely phase mismatched. Therefore, as mentioned earlier, the background was sampled with one of the ω_1 beams blocked to definitely preclude any CARS

TEMPERATURE VARIATION OF N₂ CARS SPECTRUM

$$\Delta\omega_1 = 0.8 \text{ CM}^{-1}$$

$$\Delta\omega_2 = 130 \text{ CM}^{-1}$$

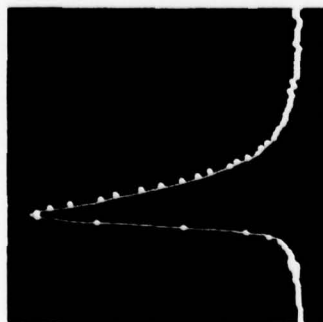
$$\text{SLIT} = 0.75 \text{ CM}^{-1}$$



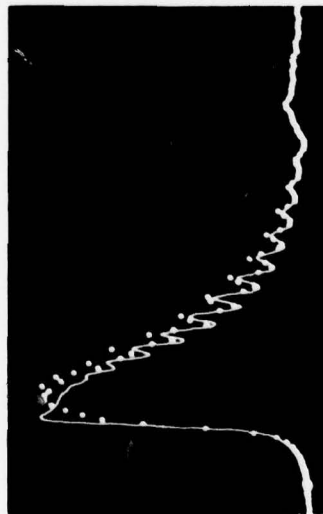
N₂ CARS SIGNATURES IN SOOTING FLAME

HMM, RMM, T(K)

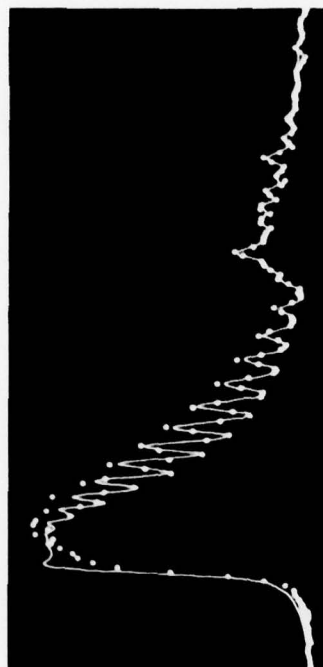
(A) 36, 8, 600



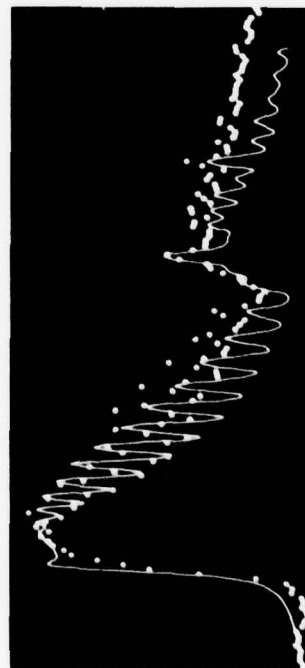
(B) 45, -4, 1400



(C) 12, 4, 1900



(D) 12, 2, 2300



(E) 1, 0, 800

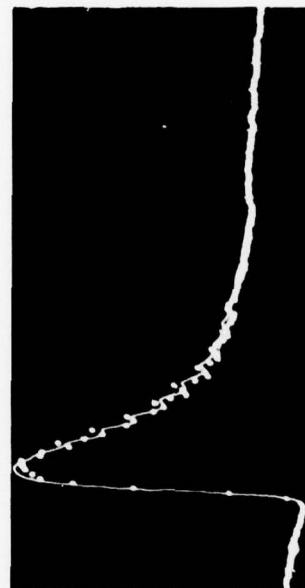


FIG. 16

generation. While the computer fits shown in Fig. 16 are generally very good, there is a discrepancy between theory and experiment in the vicinity of the $v=0+1$ band peak. The experimental signature tends to be more rounded and does not display the sharp peak predicted by theory. This discrepancy would be removed by employing slightly smaller homogeneous linewidths for the Q-branch transitions in this region. Use of smaller linewidths for all transitions would, however, lead to higher inferred temperatures, at some points in excess of the adiabatic flame temperature as pointed out earlier. It is also possible that the discrepancy results from a contribution due to collisional narrowing. The low quantum number Q-branches overlap to some extent, and it may not be strictly valid to treat these transitions as independently broadened (Ref. 26). A nonadditivity effect arising from the overlap of small J transitions may be making a small contribution to the experimental signatures. The present theoretical model does not take this phenomenon into account.

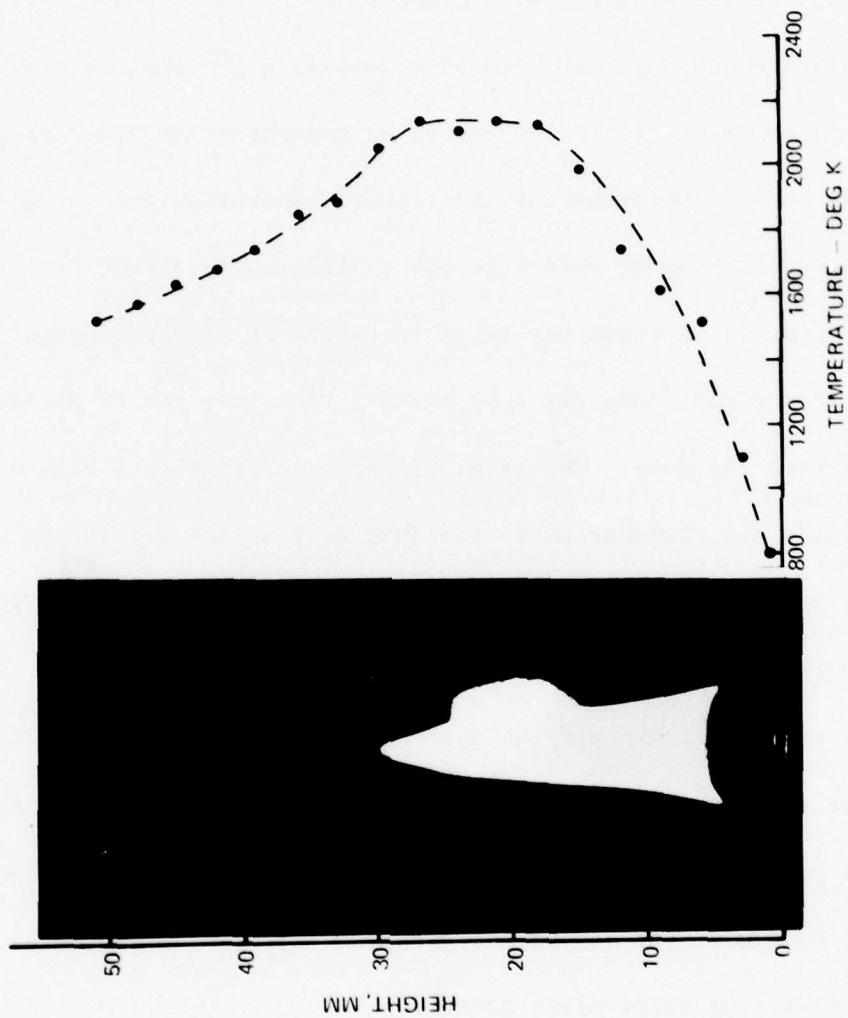
The signature shown in Fig. 16e is very interesting. The measurement was made on the centerline of the burner just 1 mm above the propane exit plane. Recall that the propane issues from a 12.7 mm I.D. tube. Experimentally the N_2 signal was found to be quite strong. From the shape of the spectrum destructive interference is apparent, indicating the importance of the background nonresonant susceptibility. To achieve the computer fit a self-consistent mixture-weighted nonresonant susceptibility was employed. In the absence of nonresonant susceptibility data on propane and water vapor, the nonresonant susceptibilities of propane and water were assumed to be equal to those of

ethane and methane respectively (Ref. 27). In actuality, the nonresonant susceptibility for the fuel dominates the susceptibility, making the calculation somewhat insensitive to the actual concentrations of the other species. The best computer fit occurred at a temperature of 800°K and a 15.5% concentration of N₂. Since propane would probably possess a χ^{nr} somewhat larger than ethane based on its size, the actual N₂ concentration would probably be somewhat lower. Nevertheless significant concentrations of N₂ are present just above the propane exit tube plane, indicating strong diffusion.

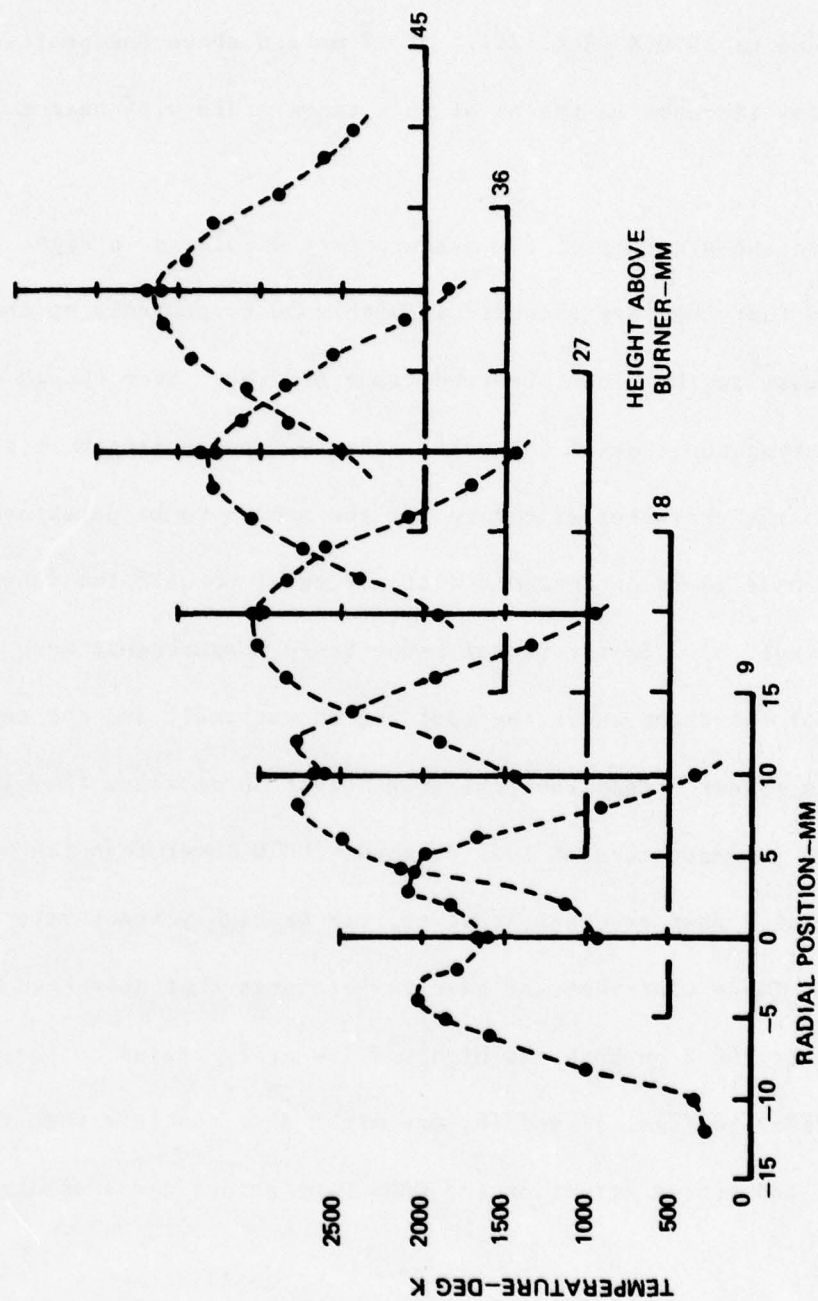
In Fig. 17 is shown the axial variation of temperature in the sooting flame with height above the tube burner. The fuel gas is already quite warm upon exiting the tube. The axial temperature rises to a peak of 2150°K in a little over one diameter above the fuel exit at the flow rates employed and remains nearly constant for about 9 mm before declining. The start of the decline is rather abrupt. The flame photographs also shows an abrupt contraction in the soot luminosity at about the same height. The sudden change in behavior is apparently caused by soot burnup in this region. Above the readily visible portion of the flame, the flame is still quite hot as seen. The luminosity diminishes due to the disappearance of the soot and not a cooling of any remaining particulate matter.

In Fig. 18 radial profiles of temperature are displayed at five different heights above the burner. The character of the diffusion flame is clearly evident. At 9 mm above the burner, the flame is nearly 500 K cooler on axis than at the 5 mm radial location where the fuel and air diffuse together and

AXIAL TEMPERATURE VARIATION IN LAMINAR PROPANE DIFFUSION FLAME



RADIAL TEMPERATURE PROFILES IN LAMINAR PROPANE DIFFUSION FLAME



react. At 18 mm some dip on the axis is still apparent. At 2 mm off the axis, the CARS temperatures indicate that the flame reaches the adiabatic flame temperature of 2250°K (Ref. 21). At 27 mm and above the profiles are smooth with a slow decrease in the axial peak temperature with height above the burner.

As to the accuracy of the measurements displayed in Figs. 17 and 18, it is suspected that they are accurate to within 50 K, probably on the high side as was the case in the clean premixed flame studies. Even though soot vaporization occurs during the time of the pulse, the 10^{-8} pulse length is considerably less than the characteristic time for the medium to be perturbed, i.e., the time for heat to be conducted a distance equal to half the interparticle spacing (Ref. 5). Soot reversal temperature measurements were performed near the tip of the flame where the soot region was small and the temperature gradients modest. Soot reversal at a height 30 mm above the flame at 5000 Å indicated a temperature of 1875°K, about 200°K lower than the CARS temperature measurement. Soot reversal, however, can be highly inaccurate as shown in Ref. 28. There soot reversal gave temperatures that disagreed with sodium line reversal by 200 K on both the high and low side. Based on the smoothness of the profiles in Figs. 17 and 18, one might also conclude that the presence of the soot had little effect on the CARS temperature measurements.

TURBULENT SOOTING FLAME STUDIES

In attempting to evaluate the practical feasibility of CARS short of full scale testing in an actual combustor, two potential jeopardies are foreseen, namely, the effect of soot particulates and the effect of turbulence. To this point, this report has focused on the former. To investigate turbulence effects, albeit on a small scale, single pulse CARS generation was examined in a temporally unsteady flame. In addition, the effect of turbulent distortions to the incident pump and Stokes beams on CARS generation was studied.

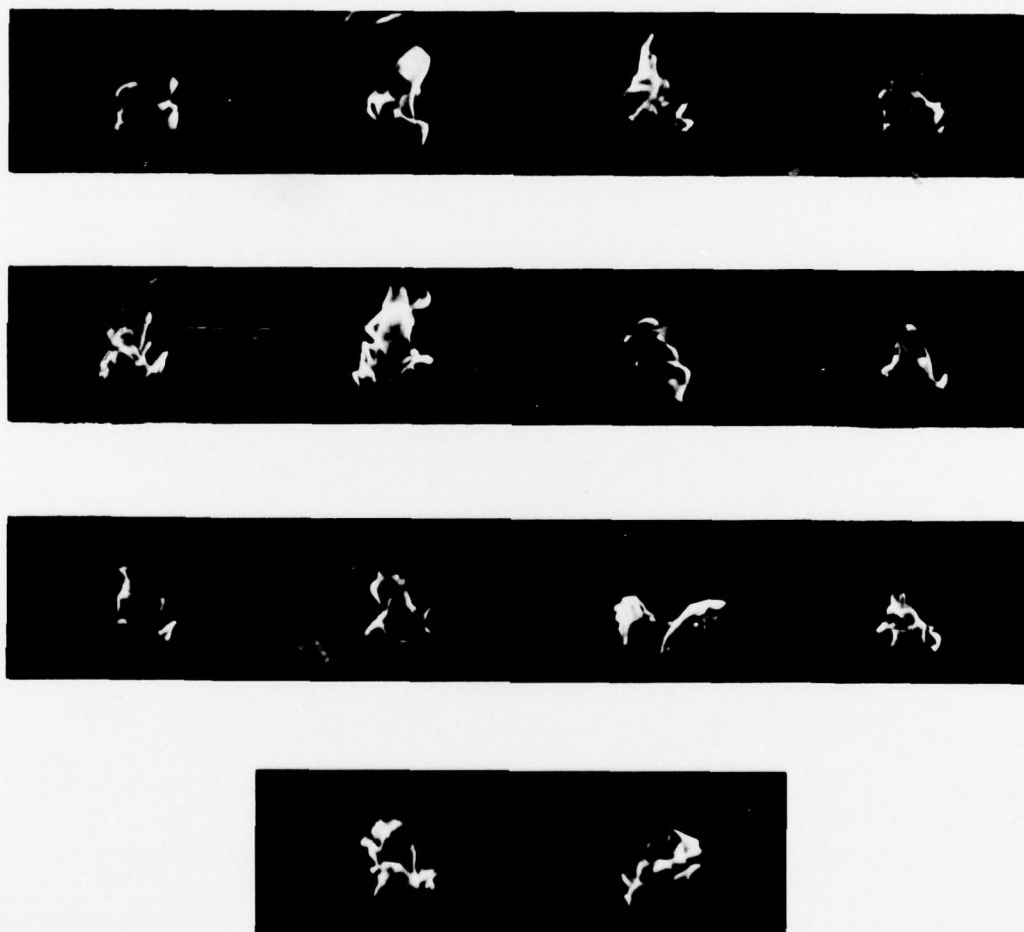
Turbulence effects are of concern in CARS generation from both a defocusing and steering standpoint. Turbulent density and temperature fluctuations cause variations in the refractive index through the region the incident beams must propagate before wave mixing occurs at the desired measurement point. As the optical path of each ray comprising the beam varies, the beam may steer and/or defocus. This, in turn, may cause the intensity of the beams to vary at the intersection (i.e., measurement) point, cause the measurement point to move, or cause the beams to miss intersecting altogether. Since the CARS signal strength is intensity dependent, defocusing and steering (so that the beams do not intersect at maximum intensity product) will cause a diminution in the CARS signal strength. For most thermometry, which depends on the spectral shape of the CARS signal, this effect is not severe as long as the CARS signal is detectable with adequate photon statistics. Spatial resolution may be degraded however. For density determinations which derive from CARS spectral shapes

(Ref. 29), the same is also true. For density determination, which derive from the intensity of the signal, such phenomena may lead to erroneous measurements. However CARS reference legs after the measurement location may serve to indicate whether a problem exists in this regard and may also provide a means of normalizing the signal to account for such effects.

In crossed-beam laser anemometry longitudinal phase variations can lead to erroneous velocity measurements (Ref. 30). This is not a problem in CARS in that, for multimode beams, there is no longitudinal phasing required, other than that the beams be temporally overlapped. Since light can traverse a distance on the order of several wavelengths in $0 (10^{-14} \text{ sec})$, there is very little possibility that refractive index fluctuations can cause any temporal separation of the interacting pulses. What is of concern are transverse phase variations across the laser beam cross section, linear variations leading to steering, and quadratic to focusing/defocusing. For propagation through small scale turbulence, i.e., a turbulence scale size small compared to the beam cross section, the transverse phase variations should pretty much average out and there should be little effect other than some defocusing due to the rms phase ripple introduced. What is of concern are large scale aerodynamic phenomena which cause substantial refractive index variations across the beam cross section. This is the case of convoluted phase boundaries, in Weinberg's nomenclature (Ref. 30), e.g., beam propagation tangential to regions of high shear. For this reason, the previously described coannular burner was employed at much higher flow rates than for the laminar flame studies. This led to a highly swirled sooting flame, almost cyclonic in appearance as seen in Fig. 19.

TURBULENT, SOOTING FLAME PHOTOGRAPHS

(500 μ SEC EXPOSURE TIME)



The figure displays photographs of the flame taken with a 500 μ sec exposure time. The highly swirled, turbulent nature of the flame is readily apparent. The flame was operated at flowrates corresponding to mean axial mass flow velocities of 67 cm/sec for the air and 7 cm/sec for the propane.

In a first series of tests, BOXCARS was generated from N_2 in room air and monitored on the boxcar averager. The effect of placing the highly swirled flame in the pump and/or Stokes beams prior to the CARS generation zone, i.e., beam intersection, was studied. Referring to Fig. 14, the flame can be placed so that just one ω_1 pump component, or the other ω_1 pump component and the adjacent ω_2 Stokes beams together, or all three beams are affected. Placing the flame in the singular pump beam component resulted in about a 40 percent decrease in the CARS signal. Placing the flame in the singular pump and Stokes components resulted in about a 50 percent decrease. Clearly, turbulent phase distortions in one leg do affect the CARS generation efficiency. However, if the flame was placed in all three incident beams, the CARS signal dropped by only 14 percent. Placing the flame after the intersection point decreased the signal by nearly 10 percent. In such a situation the CARS generation efficiency is not affected; the CARS beam experiences some degree of steering. After the dispersing prism the CARS beam travels nearly one meter before being focused down onto a 200 micron wide slit. Thus, some of the signal loss, when the flame is placed before the intersection point, is probably due solely to steering of the signal beam and not reflective of decreased CARS generation efficiency. These tests illustrate that large scale turbulent flame eddies do affect the CARS generating efficiency, but the effect (from small scale flames) appears tolerable.

In a second series of experiments, single pulse CARS generation was examined from the highly turbulent flame. Before displaying these data, Fig. 20 presents a comparison of single pulse (10 nanoseconds) and averaged CARS spectra from the laminar sooting flame studied earlier. A single CARS pulse was captured using a shutter set for 90 milliseconds aperture. Because the laser operates at 10 Hz, the capture of only a single pulse is guaranteed and with high probability. As seen the agreement between the single pulse and averaged spectra is fairly good. The single pulse spectrum is not as smooth as the average and reflects a slight degree of irregular structure on the broadband dye laser spectrum, i.e., the dye spectrum is not perfectly smooth. The slight amount of fine structure, on the order of ± 10 percent, averages out over many pulses. At the high spatial resolution, ~ 1 mm, and spectral resolution, 0.75 cm^{-1} , employed, the CARS signals are just detectable with good photon statistics from hot N_2 in atmospheric pressure flames. Recall however that the total energy out of the laser is only ~ 200 millijoules. This demonstrates that single pulse CARS thermometry can be performed with laser pulse energies about an order of magnitude lower and at repetition rates an order of magnitude higher than is possible for spontaneous Raman scattering with present day commercially available, laser sources.

Single pulse thermometry was performed in the turbulent flame situation at several locations over the double tube burner as seen in Fig. 21. These spectra were recorded at an ω_1 crossing half-angle of about 2 deg, corresponding to

SINGLE PULSE BOXCARS THERMOMETRY

LAMINAR PROPANE DIFFUSION FLAME

(A) SINGLE PULSE



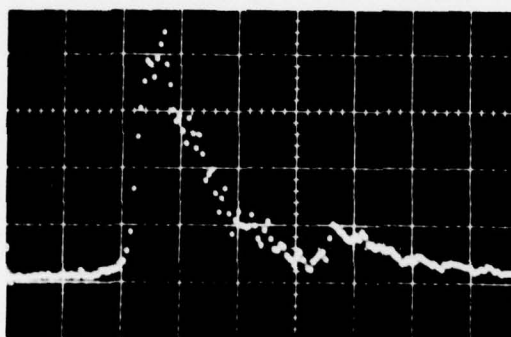
(B) AVERAGED



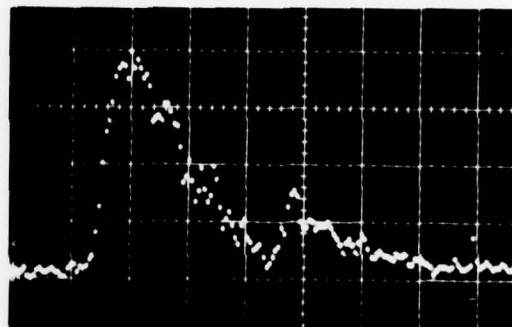
CAR SIGNATURES FROM TURBULENT, SOOTING FLAME

OUTER EDGE OF INNER FUEL TUBE

1/26/79-9

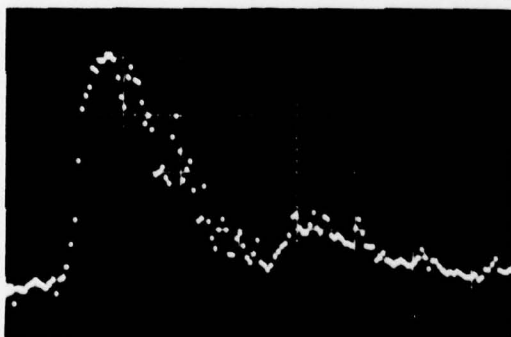


1/26/79-10b

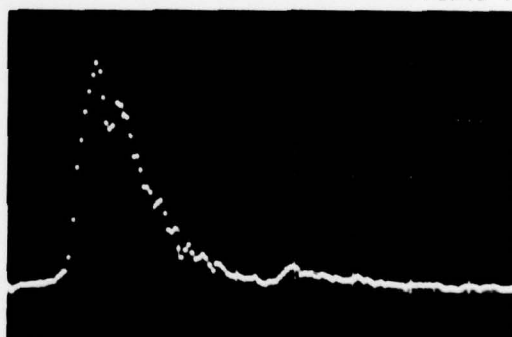


OUTER FLAME EDGE

1/26/79-15

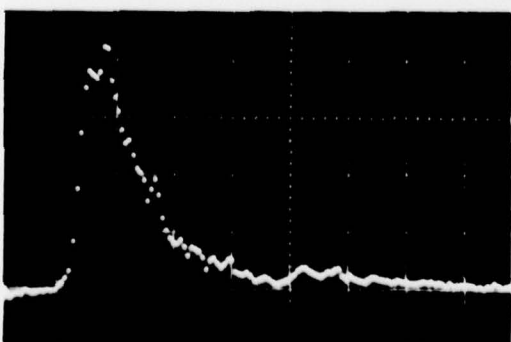


1/26/79-16

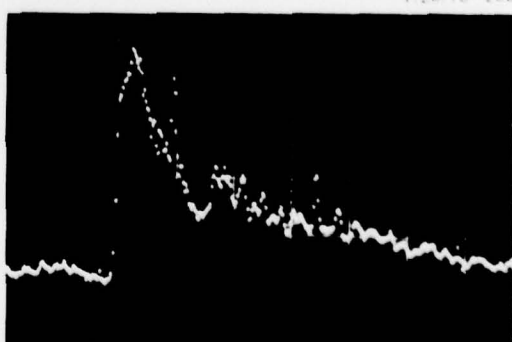


FLAME CENTER

1/26/79-21



1/26/79-23b



about a 3 mm spatial resolution. This is tolerable for the turbulent flame studies since the flame is considerably larger in scale when swirled relative to laminar operation. CARS spectra were recorded in high shear regions at the edges of both the inner and outer tubes and on the burner centerline. Figure 21 displays two examples of single pulse CARS spectra at each location at different temperatures. As can be seen the spectra are of fairly good quality and demonstrate successful CARS generation in a highly turbulent flame. The one centerline spectrum is interesting; the destructive interference seen in the N_2 spectrum is indicative of a locally high propane concentration at the particular instant of measurement.

The turbulent flame work presented in this section is quite encouraging in regards to the practical feasibility of CARS. However, these studies were limited to a relatively small scale turbulent flame, i.e., ~ 3 cm dia, which could be conveniently and safely operated in a laboratory. CARS flame studies in larger scale turbulence and/or turbulence over larger physical dimensions are, based upon the foregoing, the next logical step in the assessment of the practical utility of CARS. Investigations in real combustors or close simulations thereof are currently planned at a number of laboratories (Ref. 31) in 1979.

CONCLUSIONS

Successful CABS generation has been demonstrated, with both excellent spatial and temporal resolution in highly sooting, laminar and turbulent, propane-fueled diffusion flames. Based upon these investigations, CARS appears extremely promising for the diagnostic probing of practical combustion processes. A logical next step in the development of CARS is to examine its practical feasibility in full-scale combustor testing.

REFERENCES

1. M. Lapp and C. M. Penney: Laser Raman Gas Diagnostics. Plenum Press, New York, 1974.
2. A. C. Eckbreth: Laser Raman Thermometry Experiments in Simulated Combustor Environments. pp. 517-547 in B. T. Zinn, Ed.: Experimental Diagnostics in Gas Phase Combustion Systems. AIAA, New York, 1977.
3. A. C. Eckbreth: Applicability of Laser Raman Scattering Diagnostic Techniques to Practical Combustion Systems. Project SQUID Technical Report UTRC-4-PU, October 1976.
4. A. C. Eckbreth: Effects of Laser-Modulated Particulate Incandescence on Raman Scattering Diagnostics. J. Appl. Phys., Vol. 48, pp. 4473-4479, November 1977.
5. A. C. Eckbreth, P. A. Bonczyk and J. F. Verdick: Laser Raman and Fluorescence Techniques for Practical Combustion Diagnostics. Appl. Spect. Revs., Vol. 13, pp. 15-164, 1978.
6. W. M. Tolles, J. W. Nibler, J. R. McDonald and A. B. Harvey: A Review of the Theory and Application of Coherent Anti-Stokes Raman Spectroscopy (CARS). Appl. Spect., Vol. 31, pp. 253-272, 1977.
7. J. W. Nibler and G. V. Knighten: Coherent Anti-Stokes Raman Spectroscopy. Chapter 7, in A. Weber, Ed.: Topics in Current Physics, Springer-Verlag, Stuttgart, 1977.
8. S. Druet and J. P. Taran: Coherent Anti-Stokes Raman Spectroscopy. In C. B. Moore, Editor: Chemical and Biological Applications of Lasers. Academic Press, New York, 1979.
9. W. M. Shaub, A. B. Harvey and G. C. Bjorklund: Power Generation in Coherent Anti-Stokes Raman Spectroscopy with Focussed Laser Beams. J. Chem. Phys., Vol. 67, pp. 2547-2550, 1977.
10. A. C. Eckbreth: BOXCARS: Crossed-Beam Phase-Matched CARS Generation in Gases. Appl. Phys. Letts., Vol. 32, pp. 421-423, 1978.
11. J. W. Daily: Pulsed Resonance Spectroscopy Applied to Turbulent Combustion Flows. Appl. Opt., Vol. 15, pp. 955-960, 1976.

REFERENCES (Cont'd)

12. Y. Sasaki: Some Remarks on the Temperature Measurement of Nonisothermal Flames by the Line Reversal Technique. Jap. J. Appl. Phys., Vol. 5, pp. 439-446, May 1966.
13. W. Snelleman: Errors in the Method of Line-Reversal. Comb. and Flame, Vol. 11, pp. 453-456, December 1967.
14. R. J. Hall: CARS Spectra of Combustion Gases. Comb. and Flame, to be published in 1979.
15. J. Bendtsen: The Rotational and Rotational-Vibrational Raman Spectra of $^{14}\text{N}_2$, $^{14}\text{N}^{15}\text{N}$ and $^{15}\text{N}_2$. J. Raman Spec., Vol. 2, pp. 133-145, 1974.
16. J. J. Barrett: and A. B. Harvey: Vibrational and Rotational-Translational Temperatures in N_2 by Interferometric Measurement of the Pure Rotational Raman Effect. J. Opt. Soc. Am., Vol. 65, pp. 392-398, 1975.
17. W. Benesch, S. G. Tilford, J. T. Vanderslice, and P. G. Wilkinson: Potential Curves for the Observed States of N_2 Below 11eV. Astrophys. J., Vol. 142, pp. 1227-1240, 1965.
18. F. Rosetti: Phys. Rev., Vol. 34, p. 367, 1929 and Z Physik, Vol. 61, p. 598, 1930.
19. A. Lofthus: Spectroscopic Report No. 2. Dept. of Physik, University of Oslo, 1960.
20. A. Lofthus, and P. H. Krupenie: The Spectrum of Molecular Nitrogen. J. Phys. Chem. Ref. Data, Vol. 6, pp. 113-307, 1977.
21. A. Murty Kanury: Introduction to Combustion Phenomena. Gordon and Breach, New York, p. 131, 1975.
22. G. Herzberg: Molecular Spectra and Molecular Structure I. Spectra of Diatomic Molecules. D. Van Nostrand Co., Inc., Princeton, New Jersey, 1967.
23. This spectrum was recorded by Dr. James F. Verdick of our laboratory to whom the author is most appreciative.

REFERENCES (Cont'd)

24. S. A. J. Druet, B. Attal, T. K. Gustafson and J. P. Taran: Electronic Resonance Enhancement of Coherent Anti-Stokes Raman Scattering. *Phys. Rev. A*, Vol. 18, pp. 1529-1557, October 1978.
25. R. W. B. Pearse, and A. G. Gaydon: The Identification of Molecular Spectra. Chapman and Hall, London, 1976.
26. A. D. May, J. C. Stryland and G. Varghese: Collisional Narrowing of the Vibrational Raman Band of Nitrogen and Carbon Monoxide. *Can. J. Phys.*, Vol. 48, pp. 2331-2335, 1970.
27. W. G. Rado: The Nonlinear Third Order Dielectric Susceptibility Coefficients of Gases and Optical Third Harmonic Generation. *Appl. Phys. Letts.*, Vol. II, pp. 123-125, 1967.
28. G. Kuhn, and R.S. Tankin: Spectroscopic Measurements to Determine Temperature and Carbon Particle Size in an Absorbing Propane Diffusion Flame, *J. Quant. Spect. Rad. Trans.*, Vol. 8, pp. 1281-1292, 1968.
29. A. C. Eckbreth, R. J. Hall and J. A. Shirley: Investigations of Coherent Anti-Stokes Raman Spectroscopy (CARS) for Combustion Diagnostics. AIAA Paper 79-0083, AIAA 17th Aerospace Sciences Meeting, New Orleans, LA, January 1979.
30. N.-S. Hong, A. R. Jones and F. J. Weinberg: Doppler Velocimetry Within Turbulent Phase Boundaries. *Proc. Roy. Soc. London A*, Vol. 353, pp. 77-85, 1977.
31. AERE Harwell (England), Air Force Aero Propulsion Laboratory, ONERA (France) and the United Technologies Research Center.

Unclassified

SECURITY CLASSIFICATION OF THIS PAGE (When Data Entered)

REPORT DOCUMENTATION PAGE		READ INSTRUCTIONS BEFORE COMPLETING FORM
1. REPORT NUMBER UTRC-5-PU	2. GOVT ACCESSION NO.	3. RECIPIENT'S CATALOG NUMBER
4. TITLE (and Subtitle) CARS INVESTIGATIONS IN SOOTING AND TURBULENT FLAMES		5. TYPE OF REPORT & PERIOD COVERED Technical Report 1 Oct. 1977 to 28 Feb. 1979
		6. PERFORMING ORG. REPORT NUMBER
7. AUTHOR(s) Alan C. Eckbreth		8. CONTRACT OR GRANT NUMBER(s) N00014-75-C-1143
9. PERFORMING ORGANIZATION NAME AND ADDRESS United Technologies Research Center East Hartford, CT 06108		10. PROGRAM ELEMENT, PROJECT, TASK AREA & WORK UNIT NUMBERS NR-098-038
11. CONTROLLING OFFICE NAME AND ADDRESS Project SQUID Chaffee Hall Purdue University, West Lafayette, IN 47907		12. REPORT DATE March 1979
		13. NUMBER OF PAGES 68
14. MONITORING AGENCY NAME & ADDRESS (if different from Controlling Office) Office of Naval Research, Power Program, Code 473 Department of the Navy 800 No. Quincy Street Arlington, VA 22217		15. SECURITY CLASS. (of this report) Unclassified
		15a. DECLASSIFICATION/DOWNGRADING SCHEDULE
16. DISTRIBUTION STATEMENT (of this Report) This document has been approved for public release and sale; its distribution is unlimited.		
17. DISTRIBUTION STATEMENT (of the abstract entered in Block 20, if different from Report) Same		
18. SUPPLEMENTARY NOTES		
19. KEY WORDS (Continue on reverse side if necessary and identify by block number) CARS, Coherent Anti-Stokes Raman Spectroscopy, Remote Combustion Diagnostics, Laser-Soot Interaction Effects, Sooting Flame Thermometry.		
20. ABSTRACT (Continue on reverse side if necessary and identify by block number) Coherent anti-Stokes Raman spectroscopy (CARS) investigations in sooting, laminar and turbulent, propane-fueled diffusion flames are reported. For a 5320 Å pump wavelength, using a frequency-doubled neodymium laser, interferences can occur at very high soot densities. For N ₂ CARS, there are both incoherent and coherent components to the interference. The incoherent interference arises primarily from anti-Stokes fluorescence from C ₂ excited by Stokes laser absorption. The C ₂ is created by the laser vaporization of soot particulates,		

DD FORM 1 JAN 73 1473

EDITION OF 1 NOV 65 IS OBSOLETE
S/N 0102-LF-014-6601

Unclassified

SECURITY CLASSIFICATION OF THIS PAGE (When Data Entered)

Unclassified

SECURITY CLASSIFICATION OF THIS PAGE (When Data Entered)

shown to occur even on a nanosecond time scale. The coherent interference arises most probably from electronically-resonantly enhanced wave mixing in the C_2 . Fortunately, neither interference is very large. By proper experimental design, interference-free CARS spectra from flame N_2 can be obtained even at high soot densities. CARS signatures from N_2 have been employed to map the temperature field with high spatial precision throughout a small, luminous, highly sooting, laminar propane diffusion flame. Single pulse (~ 10 nanosecond) CARS thermometry has been demonstrated in various regions of a highly swirled, turbulent propane diffusion flame. Based upon these investigations, CARS continues to appear very promising for diagnostic applications to practical combustion sources.

approx.

Unclassified

SECURITY CLASSIFICATION OF THIS PAGE (When Data Entered)